https://doi.org/10.5194/egusphere-2025-4844
Preprint. Discussion started: 10 October 2025

Fluvial biofilm phosphorus entrapment shifts from intracellular to extracellular dominance along a multifactorial longitudinal river gradient

Simon Wentritt[1], Markus Weitere[1], David Kneis[2], Karla Münzner[3], Nuria Perujo[1]

[1]Helmholtz Centre for Environmental Research - UFZ, River Ecology Department, Brückstr. 3a, 39114 Magdeburg, Germany
[2]Technische Universität Dresden, Institute of Hydrobiology, Zellescher Weg 40, 01217 Dresden, Germany
[3]Lund University, Functional Ecology Unit, Department of Biology, Ekologihuset, Kontaktvägen 10, 22362 Lund, Sweden

Correspondence to: Simon Wentritt (simon.wentritt@ufz.de)

Abstract. Phosphorus (P) entrapment by biofilms can be distinguished into the intracellular P entrapment (the P uptake by microbial cells) and the extracellular P entrapment via the extracellular polymeric substances. It is unknown how these two P entrapment pathways behave in natural ecosystems in which gradients of environmental drivers such as P, labile dissolved organic matter (DOM) and light occur. Another key aspect in P dynamics at the sediment-water interface is microbial activity. Microbially mediated mineralization of DOM and microbial activity in general is suspected to be a driver of internal P mobilization from the sediments. Here we brought such expectations into a real-world context by analysing the P entrapment patterns of benthic biofilms and the P release potential from the sediments along a longitudinal gradient in a third order river in front of the background of key microbial metabolic variables. The gradient consists of increasing P availability, DOM lability and light availability.

We found a gradual shift in the dominance of P entrapment from higher intracellular P entrapment in the upstream biofilms to higher extracellular P entrapment in the downstream biofilms. This shift towards dominance of extracellular P entrapment was accompanied by an increase in the P release potential from the sediment. The increasing P release potential was also connected to high extracellular enzyme activity of alkaline phosphatase, an enzyme involved in the mineralization of P from organic compounds. We further found that a balanced ratio between intracellular and extracellular P was connected to a higher C metabolic diversity.

All this evidence suggests an influence of the benthic biofilms on P dynamics at the sediment-water interface. This research advocates for a more integrated perspective that accounts for both intracellular and extracellular biofilm-mediated processes.

1 Introduction

Phosphorus (P) and microbial life are inseparably intertwined in aquatic ecosystems as P is an essential macronutrient (Duhamel, 2024). Moreover, P is often considered a limiting nutrient for primary production in aquatic ecosystems (Correll, 1999) and plays a central role in stream eutrophication (Dodds and Smith, 2016). That means, in excess, P can severely impair water quality of freshwater ecosystems, impact food web structures and by extension aquatic biogeochemistry (Smith et al., 2006). Since P enters aquatic ecosystems mainly via diffuse terrestrial runoff, anthropogenic point sources or via the

https://doi.org/10.5194/egusphere-2025-4844
Preprint. Discussion started: 10 October 2025

groundwater (Mainstone and Parr, 2002) and is not commonly assimilated from the atmosphere, like carbon (C) or nitrogen (N), P is frequently recycled throughout its residence in aquatic ecosystems (Duhamel, 2024). A hotspot for biogeochemical processes, such as nutrient remineralization, is the benthic compartment of lotic ecosystems (Battin et al., 2016). Here, on surfaces at the sediment-water interface, complex microbial communities consisting of heterotrophs and photoautotrophs, embedded in a self-secreted extracellular polymeric matrix (EPS), also known as biofilm, govern these biogeochemical processes (Lock et al., 1984).

The special lifestyle of biofilms leaves them perfectly suited for the entrapment and cycling of nutrients and organic molecules (Fischer, 2003; Lock et al., 1984). The EPS readily adsorbs dissolved organic matter (DOM) as well as inorganic ions (Flemming and Wingender, 2010). Extracellularly adsorbed organic molecules can be metabolized by extracellular enzyme activity (EEA) expressed by the biofilm cells themselves (Sinsabaugh et al., 1991). Inorganic ions and small organic molecules adsorbed to the EPS or metabolites of EEA can be taken up intracellularly and used in biological processes (Jones and Lock, 1993; Zhou et al., 2017). This unique characteristic of biofilms, the differentiation in extracellular and intracellular entrapment, in particular of P, receives increasing attention in biotechnological applications such as bioreactors for P removal from wastewater (Xu et al., 2020).

Experimental work by Perujo et al. (2024) showed biofilms exposed to increased P concentrations in the water shifted to extracellular P entrapment as the main mode of biofilm P entrapment while the intracellular P entrapment capacity was saturated. Perujo et al. (2025) found that bioavailable C promoted intracellular P entrapment in experimental biofilms. These experimentally identified drivers, particularly the P concentrations and bioavailable C can differ greatly in the environment. This has given rise to the, as of yet untested, assumption that gradients in both of these drivers could help reveal the modes of P entrapment in natural environments.

An environment where gradients in bioavailable C and P concentrations occur, are lotic ecosystems, in particular those within anthropogenic land-use gradients. The headwaters of low order streams are often more forested leading to a low light availability and a higher reliance on allochthonous, often more recalcitrant DOM. Further downstream, the landscape typically opens up, and autochthonous, more labile DOM, like exudates from primary producers, becomes the dominant C source (Tank et al., 2010; Vannote et al., 1980). Increasing anthropological influence from headwaters to downstream reaches can increase stream water P loads (Mainstone and Parr, 2002; Weitere et al., 2021). All this leads to increasing gradients of light availability, DOM lability and bioavailable P concentrations along a stream and could subsequently impact the P entrapment patterns of biofilms. However, the link between longitudinal stream gradients and P entrapment patterns in biofilms is still unknown.

Another key aspect in P dynamics at the sediment-water interface is microbial activity (Meyer et al., 2024). Specifically, the mineralization of DOM via EEA has been related to P release potential from the sediment (EPC0) by Meyer et al. (2024). Microbially mediated mineralization of DOM is already suspected to play a role in internal P remobilization in aquatic ecosystems (Hupfer and Lewandowski, 2008). Further, experimental work showed that a tight coupling between C and P demand in biofilms exists. Under elevated soluble reactive P (SRP) concentrations, alkaline phosphatase activity (APA), an extracellular enzyme related to mineralization of organic P, decreased (Romaní et al., 2004), while the opposite happened

https://doi.org/10.5194/egusphere-2025-4844
Preprint. Discussion started: 10 October 2025

when a labile C source was provided (Oviedo-Vargas et al., 2013). Due to the importance of labile DOM as a heterotroph C source and the relationship between labile DOM availability and the extracellular P mineralization by APA, we expect that this relationship influences P entrapment patterns in biofilms (e.g. intracellular and extracellular P entrapment) as well as the potential release of P. In particular, a higher labile DOM availability could increase the APA which could influence P entrapment and the P release potential from the sediment. However, these ideas remain so far unexplored. Measures for microbial activity in general are microbial DOM mineralisation and C metabolic diversity. β-glucosidase (BG) and β-xylosidase (BX) are extracellular enzymes related to DOM mineralization for microbial C acquisition (Sinsabaugh et al., 2008). C metabolic diversity is defined as the ability of microbial communities to mineralize different C substrates (Garland and Mills, 1991) and it is already known that different C substrates present in freshwater ecosystems determine different microbial C metabolic profiles (Perujo et al., 2016; Ruiz-González et al., 2015). Thus, we expect that the ability of biofilm communities to accumulate intracellular P for biomass growth will depend, on the availability of C (through photosynthesis, i.e. light conditions) in autotrophs; and on the ability of heterotrophs to obtain bioavailable C through DOM mineralization (i.e. EEAs of BG and BX and C metabolic diversity). However, the influence of these processes on the patterns of intracellular and extracellular phosphorus entrapment is still unknown. In our study, we used the natural gradient of light availability, DOM lability and SRP availability of a German third order river to test our hypotheses:

1. Absolute extracellular P entrapment will increase along the gradient while absolute intracellular P entrapment will decrease along the gradient.
2. With a lower ratio of intracellular to extracellular P in the biofilm ($Ratio_{Pintra/Pextra}$), we expect an increase of the P release potential.
3. The microbial metabolic activity in the biofilms, inferred from the extracellular enzyme activity and C metabolic functional diversity, will change with the gradient.
4. The combination of a low C metabolic diversity in biofilms, a higher enzymatic investment into P acquisition than C acquisition and a higher relative extracellular P entrapment will all contribute to a higher overall P release potential from the sediment.

2 Methods

2.1 Study Sites

We studied a 25.7 km stretch of the Holtemme river, a third-order German river originating in the north-east Harz mountains, with a total length of 47 km. The Holtemme flows from the Harz National to the Bode river. The total size of the catchment is 278 km² (Wollschläger et al., 2017). In this study, we focused on a stretch of the river from 6.4 km to 32.1 kilometres from the source of the river (Table 1). We sampled along a longitudinal gradient of increasing DOM lability, light availability and SRP concentration from the relatively pristine, forested Steinerne Renne canyon to the open, heavily agriculturally influenced western outskirts of Halberstadt. Along the sampled river stretch, the Holtemme receives the discharge of several smaller,

https://doi.org/10.5194/egusphere-2025-4844
Preprint. Discussion started: 10 October 2025

agriculturally influenced, tributaries and the effluent of the waste water treatment plant (WWTP) of Wernigerode at 19 kilometres from the source. The WWTP outflow represents a strong point source of nutrients (Weitere et al., 2021).

Table 1: Overview over the sampling sites of the longitudinal sampling campaign. Site numbers relate to Weitere et al. (2021). The categorization relates to the immediate surroundings of the stream bed and the vegetation structure at the sampling sites. Distance refers to the distance from the source of the river. From here on, when referring to the sampling sites, the site number will be used.

Site No.	Site Name	Categorization	Latitude	Longitude	Distance [km]
3	MOBICOS Steinerne Renne	Pristine, dense foliage cover, forested, heterogenous stream bed structure	51°49′04.3″N	10°43′43.9″E	6.4
9	Wernigerode City	Urban, channelized stream bed, dense riverine woody vegetation	51°50′49.7″N	10°47′29.6″E	12.4
11	Minsleben	Rural surroundings, with tall deciduous trees as dominating riparian vegetation	51°51′48.1″N	10°49′52.8″E	16.1
13	UPS WWTP	Adjacent to several farm buildings, still relatively dense riverine vegetation	51°51′53.4″N	10°50′46.2″E	17.4
18	DS WWTP	Semi-urban, broader stream bed, tall coniferous trees along the shore	51°52′00.4″N	10°54′25.0″E	21.9
22	MOBICOS Mahndorf	Adjacent to old manor house with park-like surroundings enclosed by intensive agriculture, stream bed open with macrophytes	51°53′06.2″N	10°57′47.2″E	27.5
25	UPS Halberstadt	Heavily agriculturally influenced, artificial river bank with deep and relatively narrow river bed channel, riverine vegetation of grasses and small willow bushes	51°53′48.2″N	11°01′11.3″E	32.1

2.2 Sampling Design

The sampling took place on the 10th of October 2023 under baseflow conditions. At each sampling site, five benthic sediment samples were taken as replicates to adequately capture the natural heterogeneity at each site (n = 35). All replicates were treated separately. The sampling at each site was done along a stretch of roughly 20 m. Sediment samples from the centre of the river bed were taken with a small shovel. Surface sediment of the first two centimetres with a grain size of 1-3 mm was shovelled into clean plastic vials. Simultaneously, three surface water samples were taken at each sampling point along the stretch where the sediment samples were taken. The sampled water was filtered in situ through pre-rinsed 0.2 µm pore size nylon syringe

https://doi.org/10.5194/egusphere-2025-4844
Preprint. Discussion started: 10 October 2025

filters (0.2 µm Chromafil, Germany). The filtered samples were then divided into samples for spectroscopic DOM quality analysis, stored in acid rinsed scintillation vials, and samples for the water chemistry parameters, stored in amber glass bottles. Samples were stored in cooler boxes immediately after sampling. After the samples were taken, physicochemical parameters (Temperature, pH, conductivity and dissolved oxygen concentration) in the water column were measured in situ with a multiprobe (Multi 3630 IDS, Xylem Analytics Germany GmbH). All sampling equipment was conditioned with river water at the sampling spots before use. The cooled samples were taken to the laboratory the same day. Water chemistry samples were stored at 4 °C in the dark and analysed the next day. The samples for DOM quality were stored in the refrigerator at 4 °C in the dark for 24 hours until analysis. Sediment samples were stored at 4 °C and processed the next day. Each sediment sample was homogenized with a spatula and 1 cm^3 subsamples were used in all further analyses.

2.3 Biofilm Phosphorus Analysis

The procedure for the analysis of total P in the biofilm was adapted from Perujo et al. (2024). 1 cm^3 sediment subsamples were put into 15 mL centrifugation tubes (Conical Tubes 15 mL, Eppendorf SE, Germany) and 10 mL of Ringer's solution (Sigma Aldrich, USA) was added. The tubes were vortexed for 5 s and sonicated for 1 minute on ice. 1 mL of the biofilm extract was then pipetted into 2 mL microcentrifuge tubes and the rest of the biofilm extract was stored at 4 °C in the refrigerator until further use to inoculate the Biolog EcoPlates. The P concentration in the biofilm extract was then determined with inductively coupled plasma mass spectrometry (ICP-MS; 8800 Triple Quad, Agilent, USA) after complete digestion of the solid phase of the sample with nitric acid. Results are given in µg-P cm^{-3}.

For the determination of the extracellular P content of the biofilm we extracted the EPS according to Perujo et al. (2017). An EPS extract was prepared by placing the 1 cm^3 sediment subsamples in 2 mL microcentrifuge tubes (Eppendorf Safe-Lock Tubes 2 mL, Eppendorf SE, Germany) with 1 mL of Ringer's solution and 0.3 g of a cation exchange resin (AMBERLITE HPR1100). The sediment was then incubated for 1 hour at 250 rpm on an orbital shaker (IKA 130, IKA-Werke GmbH & Co. KG, Germany) on ice. After incubation, the microcentrifuge tubes were centrifuged for 15 minutes at 11.000 rpm at 4 °C (Centrifuge 5810 R, Eppendorf SE, Germany). 500 µL of the supernatant were pipetted into a new 2 mL microcentrifuge tube. The extract was then frozen until the measurement of the extracellular P in the biofilm via ICP-MS. Results are given in µg cm^{-3}. The intracellular P content in the biofilm was determined by subtracting the value for the extracellular P from the value of the total P in the biofilm of the respective samples.

For six samples, the measured extracellular P content exceeded the measured total P content in the biofilm most likely due to incomplete homogenization of the sediment before splitting into subsamples. These biologically nonsensical values were not used in the statistical analysis. Another sample was lost due to a handling error, resulting in a total of 28 observations for the biofilm P fractions with at least 3 observations for each sampling site.

https://doi.org/10.5194/egusphere-2025-4844
Preprint. Discussion started: 10 October 2025

2.4 Phosphorus Equilibrium Concentration

The phosphorus equilibrium concentration (EPC_0) as a proxy value for the P release potential from the sediment was determined. If the SRP concentration in the water reaches the EPC_0, no sorption of P to the sediment takes place (Jarvie et al., 2005). Therefore, high EPC_0 values indicate a P release potential from the sediment, since only at higher SRP concentrations, desorption of P from the sediment ceases and adsorption of SRP from the water column to the sediment occurs. We used a protocol adapted from DiCarlo et al. (2020), Inamdar et al. (2020), Roberts and Cooper (2018) and Simpson et al. (2019). First, for each sample, KH_2PO_4 (Chemsolute® TH Geyer GmbH & Co. KG, Germany) solutions were prepared (50 µg-P L^{-1}, 100 µg-P L^{-1}, 200 µg-P L^{-1}, 500 µg-P L^{-1} and 1,000 µg-P L^{-1}) by diluting a 30,000 µg-P L^{-1} solution with Milli-Q water accordingly to a volume of 10 mL. Then, the 1 cm^3 subsamples were placed in 15 mL centrifugation tubes. The samples were incubated for 24 h on an orbital shaker (GFL 3017, Gesellschaft für Labortechnik mbH, Germany) at 150 rpm in the dark at room temperature. After the incubation, the centrifugation tubes were centrifuged at 4000 rpm for 20 min. 5 mL of the supernatant were pipetted into fresh 15 mL centrifugation tubes and the P concentration was measured with the ICP-MS. With a linear regression of the measured concentrations versus the nominal P concentration of each replicate's dilution series, the x-intercept was determined.

2.5 Structural Biofilm Variables

Ash free dry weight of the biofilm was determined via loss of ignition. 1 cm^3 subsamples were muffled at 450 °C for 4 hours after drying at 60 °C in pre-weighed aluminium crucibles. The ash free dry weight was calculated as the difference of dry weight and ash content. EPS content of polysaccharides in the biofilm was determined as described in Perujo et al. (2017). The spectrophotometric measurement with a microplate reader (Safire², TECAN AG, Switzerland) was done after DuBois et al. (1956), based on a glucose standard curve and results are given in µg-glucose-equivalents cm^{-3}. Bacterial density was determined with the flow cytometer (Accuri C6, Accuri, USA) following a protocol based on Amalfitano and Puddu (2009). 1 cm^3 subsamples were placed in autoclaved glass vials filled with 10 mL of a detaching solution and kept at 4 °C in the dark until analysis. First the glass vials were vortexed (5 s) and shaken in the dark for 30 min at 150 rpm. The samples were then cooled to 4 degrees for 10 min. We sonicated the cooled samples on ice for a total 2 min in two cycles of 1 min each with 30 s rest time in between to not damage the cells. After that, the samples were vortexed and 1 mL of the extract was pipetted in a sterile 2 mL microcentrifuge tube. 1 mL of Optiprep density gradient medium (OptiPrep, Sigma-Aldrich, USA) was layered underneath with a syringe. The microcentrifuge tubes were centrifuged for 90 min at 14.000 rpm and 4 °C (Centrifuge 5424 R, Eppendorf SE, Germany). After centrifugation, the supernatant was pipetted into a new, clean 2 mL microcentrifuge tube and again centrifuged for 30 min at 14.000 rpm and 4 °C. Again, the supernatant was transferred into a new clean 2 mL microcentrifuge tube and vortexed (5 s). The sample was then diluted 1:100 by pipetting 4 µL of the sample volume into a clean cytometer tube and mixing with 396 µL of Milli-Q water. 4 µL of Syto13 (5 µM; Syto13, Fisher Scientific, USA) were added and the samples were incubated for 20 minutes in the dark at room temperature. After the incubation, 10 µL of a

https://doi.org/10.5194/egusphere-2025-4844
Preprint. Discussion started: 10 October 2025

homogenized bead solution (1.0 µm, 10^6 beads mL^{-1}; Fisher Scientific, USA) were added and the cytometer tube was vortexed for homogenization. The bacterial density in the homogenized sample was then measured via flow cytometry. Results are given as cells * 10^8 cm^{-3}. The chlorophyll-a concentration in the sediment (Chl-$a_{sediment}$) was determined via ethanol (90 %) extraction of the freeze-dried sediment (1 cm^3) and photometrical measurement (DIN-38409-60). The Chl-$a_{sediment}$ concentrations are given in µg cm^{-3}.

2.6 Biofilm metabolic Variables

Microbial C metabolic profiles based on carbon use were investigated via Biolog® EcoPlates™ (Biolog Inc., USA) after Freixa et al. (2016). 1 mL of the extract prepared for the determination of total P in the biofilm was diluted 1:20 with 19 mL of Ringer's solution. The plates were then inoculated with 130 µL per well of the diluted biofilm extract under sterile conditions. Then, the plates were incubated at 20 °C in the dark for 7 days. Every 24 hours, the absorbance of every well was measured at 590 nm with the microplate reader. The blank well was subtracted from every well of the same set of 31 substrate wells and the threshold for recording colour development was set to 0.05. Negative or smaller values were set to 0. To determine the average well colour development (AWCD), the area under the curve (AUC; definite integral of a fitted logistic function of the average absorbance values over time) was calculated according to Guckert et al. (1996). The Shannon index (the measure for C metabolic diversity), Shannon evenness (Evenness) and the substrate richness were calculated as the mean from 48 h to 144 h for each replicate. The community level physiological profiles (CLPP) were determined according to Perujo et al. (2020). Due to the extremely few absorbance values greater than 0 after 24 hours, we used the data from 48 h to 144 h for the analysis of CLPPs. We divided the different substrates on the Biolog EcoPlate into six different substrate guilds after Freixa Casals (2016) consisting of amino acids, amines, carbohydrates, carboxylic acids, phenolic compounds and polymers. The average well colour development of the substrate guilds was also calculated as the definite integral of a fitted curve of the average absorbance values of the substrate guilds over time.

Extracellular enzyme activity (EEA) was measured via fluorescent-linked substrates according to Romaní and Sabater (2001). We measured the activity of the hydrolytic extracellular enzymes β-D-glucosidase (EC 3.2.1.21, BG), β-D-xylosidase (EC 3.2.1.37, BX), alkaline phosphatase (EC 3.1.3.1-2, APA) and leucine-aminopeptidase (EC 3.4.11.1, LAP). The fluorescent-linked substrates were 4-Methylumbelliferyl (MUF) beta-D-glucoside for the activity of BG, MUF beta-D-xylopyranoside for the activity of BX, MUF-phosphate for the activity of APA and L-Leucine-7-amido-4-methylcoumarin (AMC) for the activity of LAP. Each fluorescent-linked substrate was dissolved in 1 mL of ether and diluted to a concentration of 10 mM with autoclaved Milli-Q water. Sediment subsamples of 1 cm^3 were placed into 15 mL centrifugation tubes, one for each enzyme assay. 4 mL of Ringer's solution were added to each subsample and 120 µL of each respective fluorescent linked-substrate were added. The centrifugation tubes were first manually mixed and then placed on an orbital shaker for 120 min at room temperature at 130 rpm in the dark. To stop the incubation, 4 mL of glycine buffer (pH 10.4) were added. The tubes were then centrifuged for 2 min at 2000 rpm. After the centrifugation, 350 µL of the supernatant were pipetted into black 96-well plates (Costar black flat bottom 96 well plates, Corning Inc., USA) and the fluorescence was measured at 365/455 (excitation-

https://doi.org/10.5194/egusphere-2025-4844
Preprint. Discussion started: 10 October 2025

/emission-wavelength) for MUF and 364/445 (excitation-/emission-wavelength) for AMC. The same procedure was used for substrate blanks (same procedure without sample material) to determine substrate auto-dissociation. To finally determine the EEA, standard curves with known MUF and AMC concentrations respectively were produced and fluorescence was measured accordingly. The results are given in µmol MUF h^{-1} cm^{-3} and µmol AMC h^{-1} cm^{-3} respectively. Logarithmic ratios of the EEA for enzymes degrading C-compounds (sum of BG and BX) to the enzymes connected to N mineralization ($ER_{C:N}$) and P mineralization ($ER_{C:P}$) respectively as well as the logarithmic ratio of N mineralization and P mineralization related enzymes ($ER_{N:P}$) were calculated after Sinsabaugh et al. (2009) to compare the microbial investment into the acquisition of C, N and P.

2.7 Water Chemistry, Foliage Cover and DOM quality

Water samples for dissolved organic carbon (DOC), dissolved nitrate (NO_3-N), dissolved bound N (DNb), total dissolved P (TP) and SRP were determined in triplicates at each sampling site. The DOC concentration was quantified via thermic-catalytic oxidation on a DIMATOC 2000 (DIMATEC Analysetechnik GmbH, Germany). NO_3-N and DNb concentrations were quantified photometrically after reduction and formation of a purple azo dye with a segmented flow analyser (Skalar Analytical, Netherlands). SRP was also determined photometrically via the ammonium molybdate method (DIN EN ISO 6878) with the segmented flow analyser. TP was determined photometrically with the ammonium molybdate method (DIN EN ISO 6878) after acid digestion with a photometer (DR 500 Hach Lange GmbH, Germany). All water chemistry variables are given in mg L^{-1} except SRP and TP which are given in µg L^{-1}.

Light availability above the river bed was determined by taking pictures of the sky with a camera at a constant distance (10 cm) above the water surface. At every sampling site, five pictures were taken to capture the variability of the vegetation cover at each sampling site. The vegetation cover was then analysed with the coveR2 package in R (Chianucci et al., 2023). The package calculates the percentage of the provided picture which is covered by vegetation. The light availability was then calculated as the difference of a sky without any vegetation (100 percent light availability) and the calculated percentages for vegetation cover of the pictures taken.

DOM quality was determined via four DOM quality proxies based on bulk optical properties. To estimate the DOM origin, we measured the fluorescence index (FI) after Cory and McKnight (2005). The DOM molecular weight was determined according to Helms et al. (2008) as the slope ratio. Here, higher values are related to lower molecular weight molecules and vice versa. For the biological index (BIX), we followed Huguet et al. (2009). Here, lower values are related to higher microbial degradation of the DOM and indicate DOM of rather terrestrial origin, while higher values relate to less degraded DOM of aquatic origin. The last DOM quality index we measured was the E2:E3-index (E2:E3, Minero et al., 2007). E2:E3 is inversely proportional to the aromaticity degree and size of DOM molecules. We measured absorbance values with a spectrophotometer (Cary 60, Agilent Technologies, USA) with 1 cm quartz cuvettes at a range from 250 nm to 400 nm. The fluorescence of the water samples was measured with a microplate reader with black flat bottom 96-well plates (FI: excitation wavelength / emission wavelength [370/470 and 370/520]; BIX: excitation wavelength / emission wavelength [310/380 and 310/430]).

https://doi.org/10.5194/egusphere-2025-4844
Preprint. Discussion started: 10 October 2025

2.8 Data Analysis

A longitudinal gradient of SRP, light availability and DOM quality in the Holtemme was already described (Weitere et al., 2021). For this study, we recharacterized the longitudinal gradient along the river. The predictor variables, namely the water chemistry data (DOC, NO_3-N, DNb, DP, and SRP), physicochemical data (pH, T°, DO and conductivity), the DOM quality proxies (FI, BIX, slope ratio and E2:E3) and the light availability were mostly highly correlated with each other and the distance from the sampling sites to the source of the river ($\rho > 0.7$). A correlation matrix of Spearman rank correlation analysis is shown in the Appendix A (Fig. A1). Benjamini-Yekutieli was used to control the type I errors due to multiple testing (Benjamini and Yekutieli, 2001). Due to the high correlation between the predictor variables and the distance from the source, it was concluded to use the distance from the source (Distance) as a suitable proxy predictor for the analysis of the response variables.

Generalized linear models (glm) based mainly on gamma distributions with log-link functions were employed to identify the patterns of P entrapment in benthic biofilms and P release potential along the longitudinal gradient. Structural biofilm variables (AFDW, bacterial density, EPS and Chl-$a_{sediment}$) were analysed the same way, except that for Chl-$a_{sediment}$ the glm was expanded for zero-inflation. The model fit was checked with Q-Q-plots of the scaled quantile residuals of the fitted data versus expected theoretical quantiles. Further, Kolmogorov-Smirnov tests, tests for over- and under dispersion and outlier tests were performed on the scaled quantile residuals.

Microbial C metabolic profiles, C substrate guild use and EEAs as well as logarithmic EEA ratios, were analysed using a one-way-ANOVA. Distance from the source was used as the explanatory variable. Homogeneity of variances for the one-way-ANOVAs was tested with Levene's test. To test for normality of residuals, Shapiro-Wilk tests were employed. The ANOVA output was then further analysed with a Tukey's Honest Significant Differences pairwise comparison as a post-hoc test. Finally, to better visualize the differences between the sampling sites, a compact letter display was employed. Community-level physiological profiles (CLPPs), based on the microbial metabolic profiles and repeated for the substrate guilds, were examined using the method described by Perujo et al. (2020). The daily absorbance data were first organized as repeated measures, treating values from all incubation times as compositional data, and their isometric log-ratios were computed. To assess significant differences in CLPPs between sites, a multivariate analysis of variance (MANOVA) using Pillai's test statistic was applied, followed by plotting CLPPs in a canonical bivariate plot (Perujo et al., 2020).

We used a multivariate principal component analysis (PCA) to analyse the relationships between the different variables covering all backgrounds in our study: environmental variables, extracellular enzymatic ratios, EPC_0, biofilm P variables, C use related variables, and structural biofilm variables. A correlation matrix for a Spearman rank correlation with the variables used in the PCA is shown in the supplementary material. Again Benjamini-Yekutieli was used to control the type I errors due to multiple testing. All statistical analysis and plots were made in R (version 4.4.0, R Core Team, 2021).

https://doi.org/10.5194/egusphere-2025-4844
Preprint. Discussion started: 10 October 2025

3 Results

3.1 Longitudinal Gradients of potential drivers: SRP, light and DOM quality

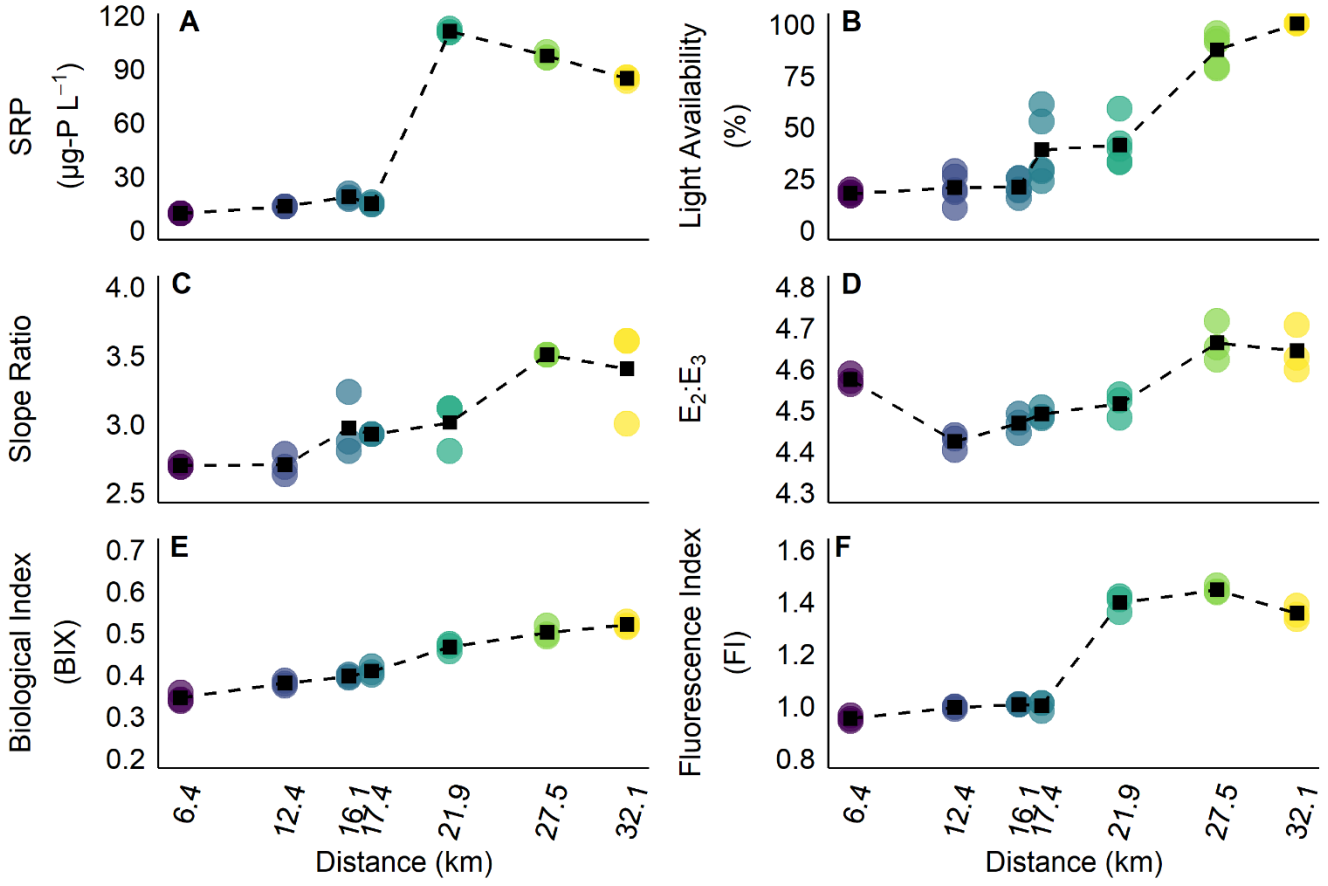

Figure 1: Longitudinal development (distance from source) of the most comprehensive explanatory variables. Black squares show the mean of the replicates at each sampling site, colours indicate the gradual increase in distance from the source. (A) SRP concentration, (B) light availability as the percentage of sky not covered by vegetation (C to F) the four DOM lability proxies slope ratio (C), E2:E3 (D), Biological index (E) and Fluorescence index (F). The value of all variables increases with the distance from the source in a significant manner ($p < 0.05$ each, Spearman rank correlation Fig. A1).

Environmental variables measured along the Holtemme river show distinct longitudinal gradients. The mean SRP concentration (Fig. 1 A) is increasing from 9 µg L^{-1} at the sampling site furthest upstream to 110 µg L^{-1} at the sampling site at 21.9 km. After this maximum, the mean SRP concentration slightly decreased to 84 µg L^{-1} at the last sampling site, which is still a 9-fold increase compared to the first sampling site. The mean light availability (Fig. 1 B) is monotonically increasing from 18 % light availability at the most upstream sampling site to 100 % light availability (no riverine vegetation) at the sampling site furthest downstream. The bulk DOM characterization based on the spectroscopic proxies shows an increase in DOM lability from the upper reach sites to the lower reach sites. The bulk DOM molecular weight is decreasing as indicated by the slope ratio (Fig. 1 C), which increased from 2.7 at the uppermost sampling site to 3.5 – 3.4 at the sampling sites furthest

https://doi.org/10.5194/egusphere-2025-4844
Preprint. Discussion started: 10 October 2025

downstream. The bulk DOM aromaticity degree initially increased from the first sampling site onward and decreased further downstream as indicated by the E_2:E_3 (Fig. 1 D). The biological index, a measure of recent autochthonous contribution to the bulk DOM, increased monotonically (Fig. 1 E) from a mean of 0.3 at the uppermost sampling site to 0.5 at the sampling site furthest downstream. The relative contribution of microbially derived DOM increased as well with distance from the source as shown by the increase of FI (Fig. 1 F) from 0.9 at the most upstream sampling site to 1.4 – 1.3 at the most downstream sampling sites. See table A1 for an overview of all measured explanatory variables.

3.2 Longitudinal patterns of biofilm P entrapment and release potential

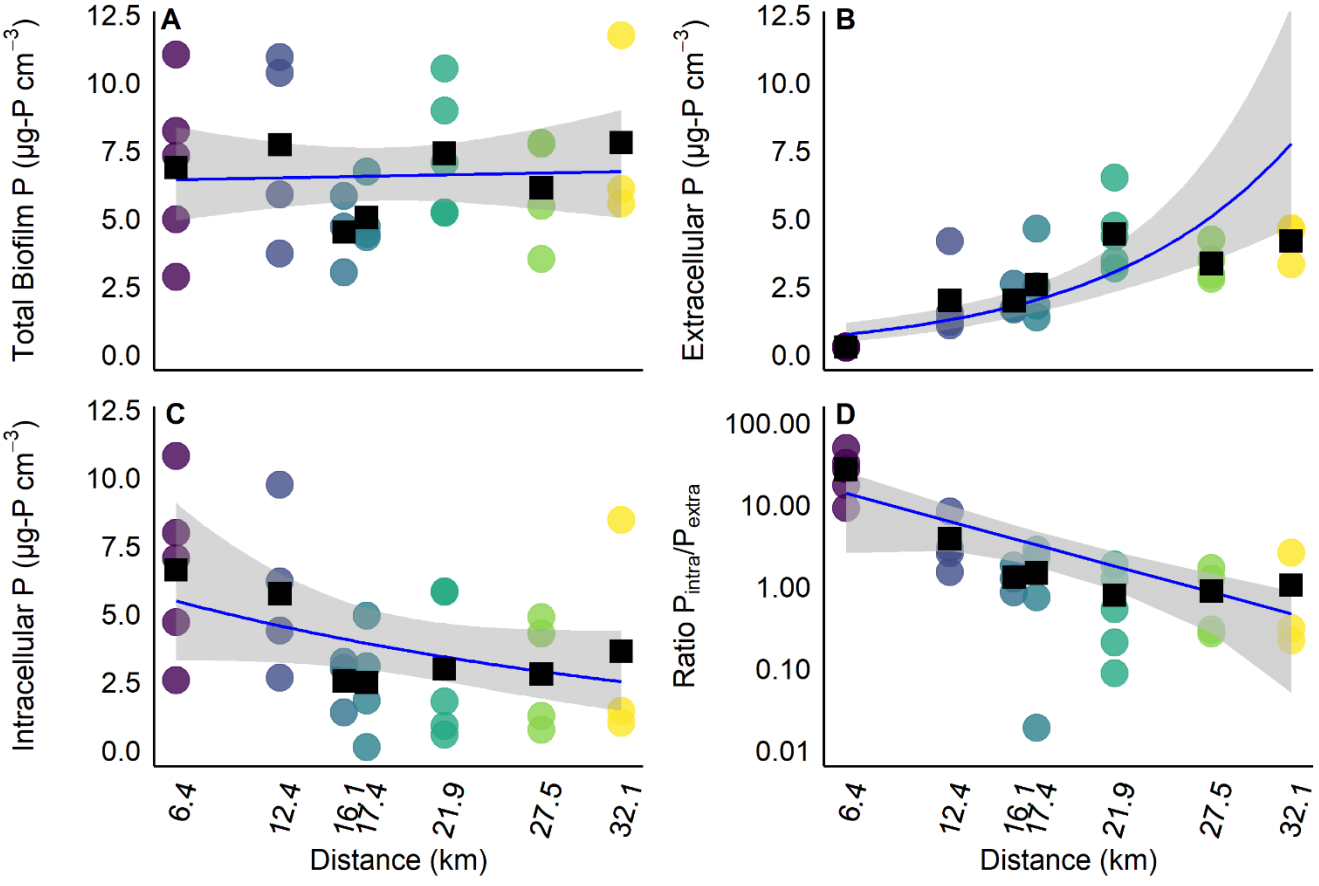

Figure 2: Longitudinal development of biofilm P patterns. Black squares show the mean of the replicates at each sampling site and circles are the raw observations. Blue regression lines represent smoothed predicted values (glm) and 95 % confidence intervals are calculated from the standard errors. The colors indicate the gradual increase in distance from the source. (A) total biofilm P concentration, (B) extracellular P concentration in the EPS, (C) intracellular P concentration and (D) ratio of intracellular to extracellular P concentrations.

Spatial patterns of P fractions in the biofilms along the stream transect revealed contrasting trends for total, extracellular, and intracellular P concentrations. The mean of the total P in the biofilm was at 6.9 µg cm^{-3} at the first sampling site and at the last

https://doi.org/10.5194/egusphere-2025-4844
Preprint. Discussion started: 10 October 2025

sampling site, it reached a maximum of 7.8 µg cm^{-3}. No significant change of the total P in the biofilm was detected with distance ($p = 0.85$, Fig. 2 A, Table B1). Extracellular P, on the other hand showed a significant increase with distance and therefore the longitudinal gradient ($p < 0.001$, Fig. 2 B, Table B1). The mean concentration increased from 0.3 µg cm^{-3} to a maximum of 4.4 µg cm^{-3} at the sampling site at 21.9 km, before decreasing to 4.2 µg cm^{-3} at 32.1 km. Intracellular P showed a noticeable but non-significant decrease with increasing distance ($p = 0.1$, Fig. 2 C, Table B1). The mean intracellular P concentration decreased from 6.6 µg cm^{-3} at 6.4 km to 3.6 µg cm^{-3} at 32.1 km, with the lowest value recorded at 17.4 km (2.5 µg cm^{-3}). The ratio of intracellular to extracellular P ($Ratio_{Pintra/Pextra}$) significantly decreased with distance ($p = < 0.001$, Fig. 2 D, Table B1), from a maximum of 26.9 to 1 at the sampling site furthest downstream.

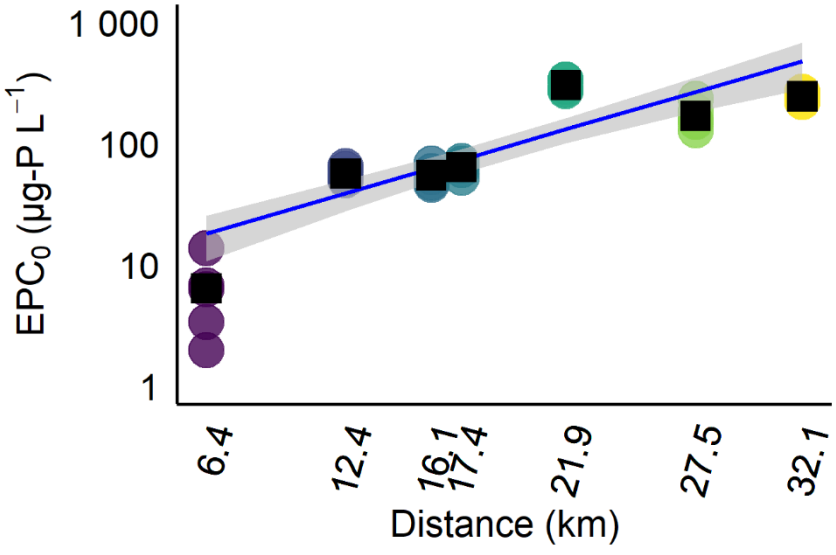

Figure 3: Longitudinal development of P release potential from the sediment. Black squares show the mean of the replicates at each sampling site and circles are the raw observations. The blue regression line represents smoothed predicted values (glm) and 95 % confidence intervals are calculated from the standard errors. Note that the y-axis is log-transformed to better visualize the trend and higher resolution of comparatively small EPC_0 values.

The EPC_0 increased significantly with distance, indicating a considerable increasing P release potential along the gradient ($p < 0.001$, Fig. 3, Table B2). Mean EPC_0 was the lowest at the most upstream sampling site with 6.4 µg L^{-1}. At the sampling site furthest downstream, the mean EPC_0 reached 245.7 µg L^{-1}.

https://doi.org/10.5194/egusphere-2025-4844
Preprint. Discussion started: 10 October 2025

3.3 Structural Biofilm Parameters

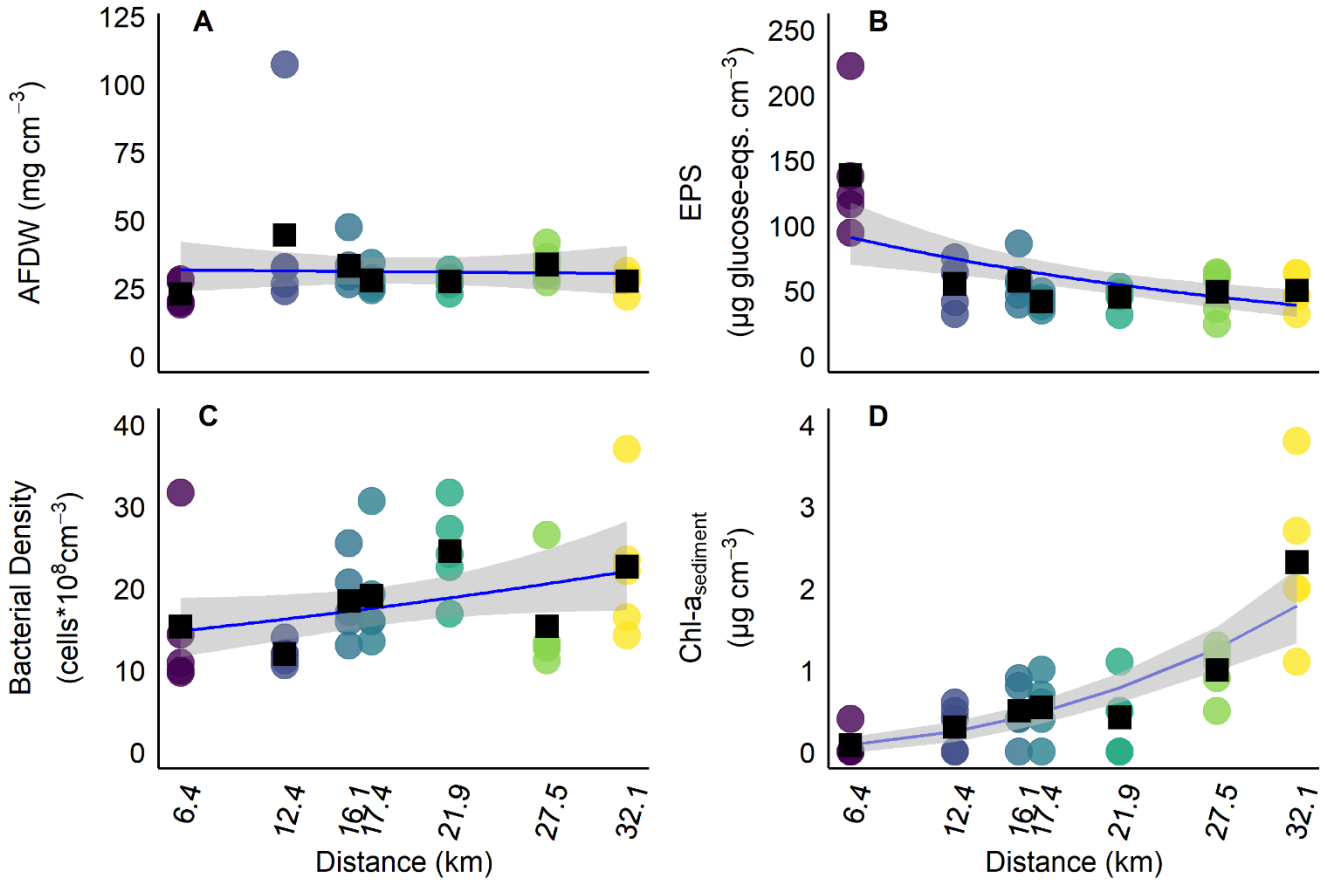

Figure 4: Longitudinal development of structural biofilm parameters. Black squares show the mean of the replicates at each sampling site and circles are the raw observations. Blue regression lines represent smoothed predicted values (glm) and 95 % confidence intervals are calculated from the standard errors. The colors indicate the gradual increase in distance from the source. (A) ash free dry weight, (B) extracellular polymeric substances as glucose equivalents, (C) bacterial density and (D) Chl-a$_{sediment}$.

Longitudinal patterns in biofilm structural and microbial variables along the stream revealed variable responses with distance, including significant trends for EPS (negative) and Chl-a$_{sediment}$ (positive), while AFDW and bacterial density showed non-significant changes. More detailed, EPS showed a significant decrease with distance ($p < 0.001$, Fig. 4 B, Table B3). The mean EPS decreased from 138.7 µg-glucose-equivalents cm^{-3} to 50.2 µg-glucose-equivalents cm^{-3} at the most downstream sampling site. Results from Chl-a$_{sediment}$ showed a significant increase with distance ($p < 0.001$, Fig. 4 D, Table B3). From the most upstream sampling site to the most downstream sampling site we found an increase in mean Chl-a$_{sediment}$ from 0.1 µg cm^{-3} to 2.3 µg cm^{-3}. The AFDW showed no specific trend ($p = 0.87$, Fig. 4 A, Table B3). At the first sampling site, the mean AFDW was at 23 mg cm^{-3} and at the last sampling site, the mean AFDW was at 27 mg cm^{-3}, fluctuating in between. Bacterial density showed a non-significant increase with distance ($p = 0.06$, Fig. 4 C, Table B3). The mean bacterial density ranged from 15.3 cells*10^{8} cm^{-3} at the uppermost sampling site to 22.7 cells*10^{8} cm^{-3} at the sampling site furthest downstream.

https://doi.org/10.5194/egusphere-2025-4844
Preprint. Discussion started: 10 October 2025

3.4 Biofilm metabolic profiles

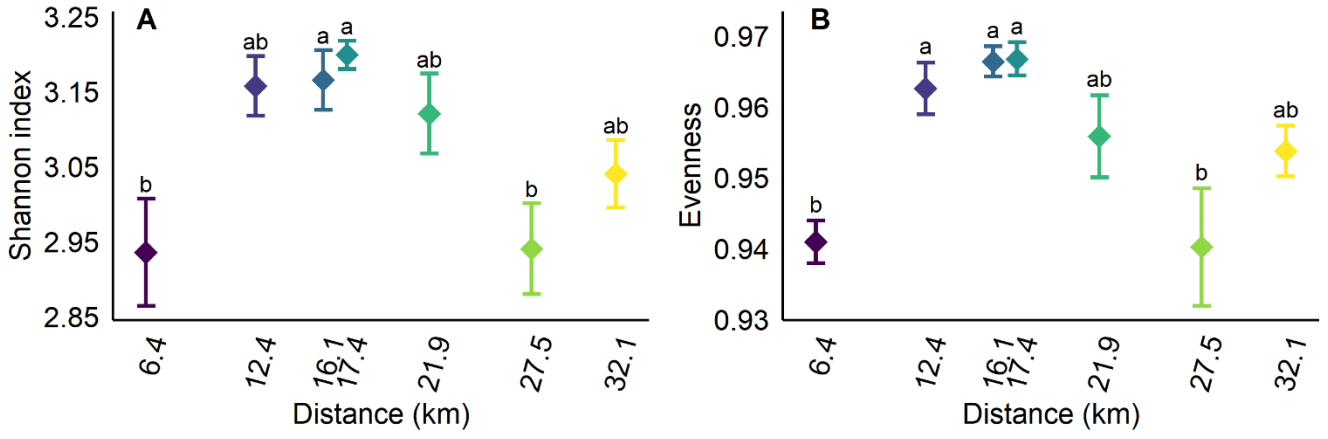

Figure 5: Longitudinal patterns of diversity indices calculated from microbial C substrate use. Diamonds represent mean values and error bars show the standard error of the mean. Mean values sharing a common letter are not significantly different from each other according to a Tukey's honest significance test at a 5% level of significance. The colours indicate the gradual increase in distance from the source. (A) Shannon index and (B) Shannon evenness.

The mean Shannon index at the uppermost sampling site was 2.9; it then increased to a maximum of 3.2 at the sampling site at 17.4 km. Then the Shannon index decreased again to a mean of 2.9 at the sampling site at 27.5 km. At the most downstream site, the mean Shannon index was at 3.0. The Shannon index of the biofilms at the uppermost sampling site and the sampling site at 27.5 km were significantly lower than the Shannon index at the two middle reach sites at 16.1 km and 17.4 km ($p < 0.05$, Fig. 5 A, Table C1). The evenness (Shannon evenness for C substrate use) followed a similar pattern. The uppermost sampling sites had a mean substrate use evenness of 0.94 which increased at the middle reach sites to a maximum mean of 0.97 at the sampling site at 17.4 km. The evenness decreased again to 0.94 at the sampling site at 27.4 km to increase again at the last sampling site to 0.95. The evenness at the uppermost sampling site and the sampling site at 27.5 km were both significantly lower than at all three middle reach sites from 12.4 km to 17.4 km ($p < 0.001$) while the other sampling sites showed no statistically different evenness (Fig. 5 B, Table C1). CLPPs based on the guild level substrate use (Table C2, Fig. C2) and based on the non-clustered substrate use (Table C3, Fig. C3) can be found in the supporting information. CLPPs revealed distinguishable patterns for C use depending on the river reach.

https://doi.org/10.5194/egusphere-2025-4844
Preprint. Discussion started: 10 October 2025

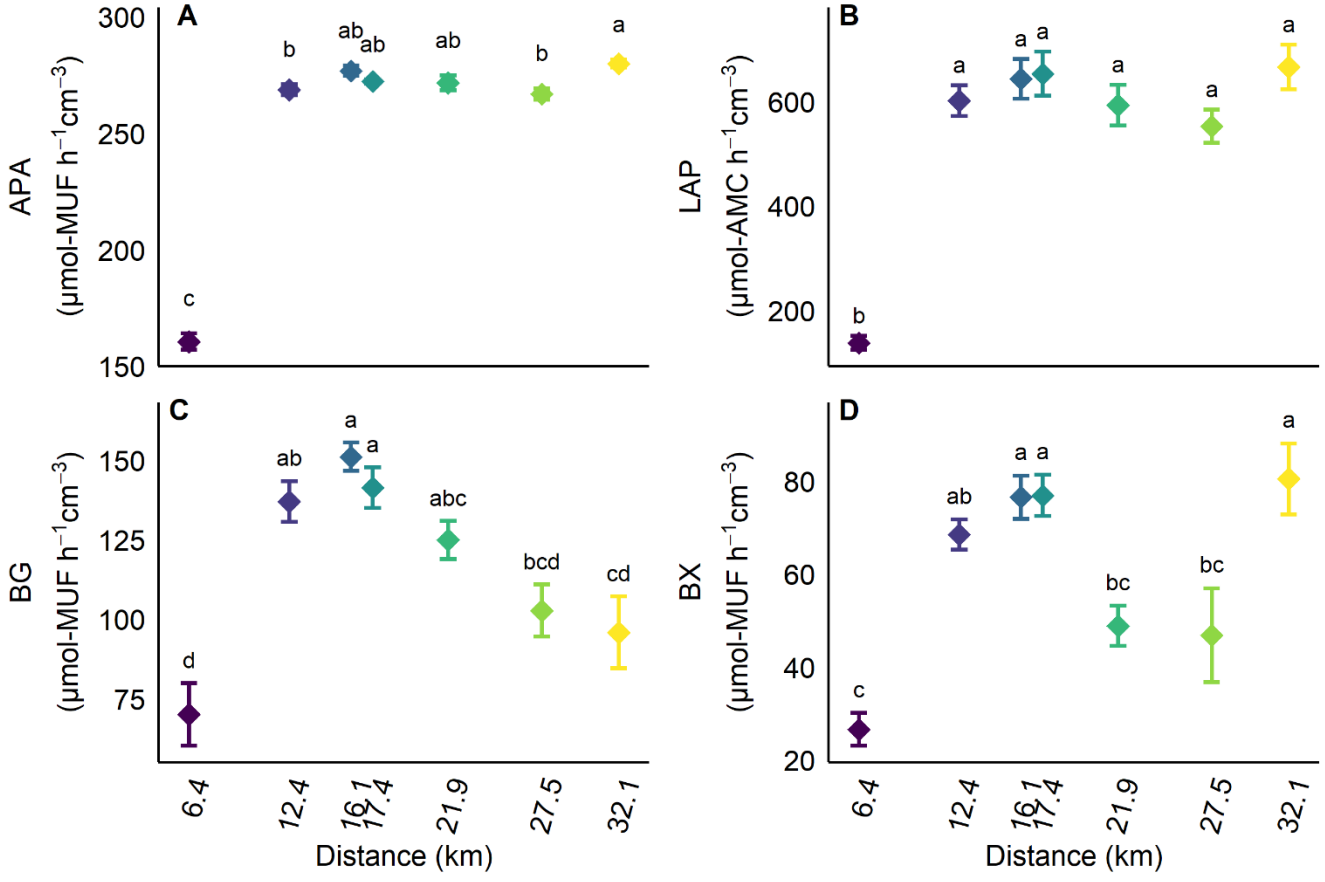

Figure 6: Longitudinal patterns of extracellular enzyme activities. Diamonds represent mean values and error bars show the standard error of the mean. Mean values sharing a common letter are not significantly different from each other according to a Tukey's honest significance test at a 5% level of significance. The colors indicate the gradual increase in distance from the source. (A) alkaline phosphatase activity, (B) leucine-aminopeptidase activity, (C) β-D-glucosidase activity and (D) β-D-xylosidase activity.

APA was the lowest at the uppermost sampling site with 160 µmol-MUF h^{-1} cm^{-3} and significantly lower than at all other sampling sites ($p < 0.001$). The APA increased greatly further downstream to a maximum mean of 280 µmol-MUF h^{-1} cm^{-3} at the most downstream sampling site. The most downstream site also had a significantly higher APA than the two sites at 12.4 km and 27.5 km ($p < 0.05$, Fig. 6 A, Table C5). LAP showed a similar pattern as APA with the uppermost sampling site having a significantly lower LAP than all the other sampling sites ($p < 0.001$). At the uppermost sampling site, the LAP was 137 µmol-AMC h^{-1} cm^{-3} and it increased to a maximum mean LAP of 666 µmol-AMC h^{-1} cm^{-3} at the most downstream sampling site (Fig. 6 B, Table C5). For the BG, the pattern was more complex (Fig. 6 C, Table C5). The uppermost sampling site at 6.4 km exhibited the lowest mean BG with 70 µmol-MUF h^{-1} cm^{-3}, significantly lower than the sampling sites from 12.4 km to 21.9 km ($p < 0.001$). The mean BG was the highest at the sampling points from 12.4 km to 17.4 km with mean enzyme activities ranging from 137 µmol-MUF h^{-1} cm^{-3} to 151 µmol-MUF h^{-1} cm^{-3}. Further downstream the mean BG decreased to 96 µmol-MUF h^{-1} cm^{-3} at the sampling site furthest downstream. The sampling sites at 27.5 km and 32.1 km had both a

https://doi.org/10.5194/egusphere-2025-4844
Preprint. Discussion started: 10 October 2025

significantly lower BG than the middle reach sampling sites from 16.1 km to 17.4 km ($p < 0.001$) and the most downstream site showed a significantly lower BG than the sampling site at 12.4 km ($p < 0.05$). Mean BX behaved similarly to BG from the first sampling site to the sampling site at 17.4 km with a strong increase from 27 µmol-MUF h^{-1} cm^{-3} to 77 µmol-MUF h^{-1} cm^{-3} (Fig. 6 D, Table C5). The mean BX decreased at the sampling sites at 21.9 km and 27.5 km to 49 µmol-MUF h^{-1} cm^{-3} and 47 µmol-MUF h^{-1} cm^{-3} respectively. At the last sampling site, the mean BX reached the highest value with 80 µmol-MUF h^{-1} cm^{-3}. The sampling sites at 16.1 km, 17.4 km and 32.1 km all showed a significantly higher BX than the sampling sites at 6.4 km, 21.9 km and 27.5 km ($p < 0.05$). Additionally, the middle reach sampling site at 12.4 km had a significantly higher BX than the uppermost sampling site ($p < 0.001$). Results for the analysis of logarithmic EEA ratios can be found in the supporting information (Figure C5, Table C5).

https://doi.org/10.5194/egusphere-2025-4844
Preprint. Discussion started: 10 October 2025

3.5 Link between biofilm P and microbial metabolic variables

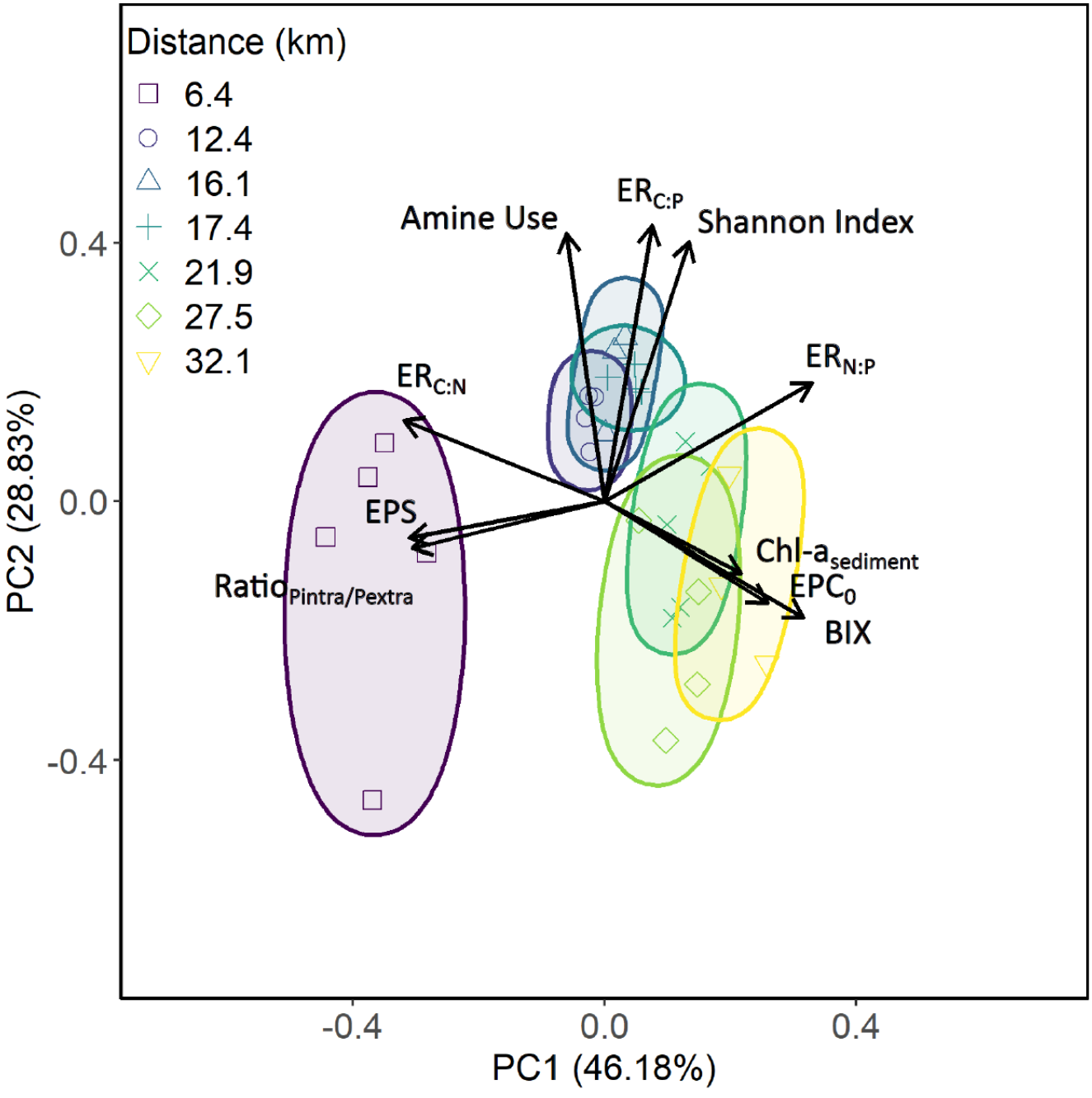

Figure 7: Multivariate principal component analysis (PCA) of EPC_0, $Ratio_{Pintra/Pextra}$, EPS, $ER_{C:P}$, $ER_{C:N}$, $ER_{N:P}$, Shannon index, Amine use, Chl-$a_{sediment}$ and BIX. Ellipses are for visual aid only; colours and shapes refer to the different sampling sites along the longitudinal stream gradient and indicate the gradual increase in distance from the source. Loading arrow length indicates the

https://doi.org/10.5194/egusphere-2025-4844
Preprint. Discussion started: 10 October 2025

contribution of the variable to the principal component analysis and direction indicates the association of the variable to the principal components.

A PCA was performed to visualize overarching patterns between the different variables. The first two principal components explain 74 % of the variation (Fig. 7). PC1 was mainly associated with variables being directly influenced by the longitudinal stream gradient. PC2 meanwhile was associated with biofilm metabolic variables. A clear separation into three distinct clusters along the x-axis was found. This separation was governed by the variables that followed the longitudinal gradient. The uppermost sampling site is characterized by a high $Ratio_{Pintra/Pextra}$, high EPS content and a high $ER_{C:N}$. Conversely, there is the cluster of the sampling sites downstream of 21.9 km. These sampling sites and their placement on the biplot are governed by higher values of the environmental variables forming the gradient in the river such as the BIX, as well as by higher EPC_0 and higher Chl-$a_{sediment}$. The three middle reach sampling sites from 12.4 km to 17.4 km are placed in between on the x-axis. Their placement though is governed by the PC2 and the increased metabolic variables which changed largely independent from the longitudinal river gradient. These three sites are clustered higher up on the y-axis, with a higher $ER_{C:P}$, a higher Shannon index and a higher Amine use.

Regarding the relationships between stoichiometric extracellular enzyme ratios and the other variables in the PCA, we found that the $ER_{C:P}$ was significantly positively correlated with the Amine use ($p < 0.05$, $\rho = 0.64$) and the Shannon index ($p < 0.001$, $\rho = 0.76$). The $ER_{C:N}$ was significantly negatively correlated with BIX ($p < 0.001$, $\rho = -0.7$) and EPC_0 ($p < 0.001$, $\rho = -0.77$) and significantly positively correlated with the $Ratio_{Pintra/Pextra}$ ($p < 0.05$, $\rho = 0.67$), thus the gradient forming variables as well as variables responsive to the gradient. The $ER_{N:P}$ was significantly positively correlated with the Shannon index ($p < 0.001$, $\rho = 0.76$, Fig. D1).

4 Discussion

4.1 Increasing gradient of light DOM lability, SRP concentration and light availability in the Holtemme River

The longitudinal gradient of increasing DOM lability, increasing SRP and increasing light availability in the Holtemme River is already well established (Kamjunke et al., 2019; Weitere et al., 2021). Our own assessment reiterates that bulk DOM can be characterized as relatively recalcitrant in the upper reaches and as relatively labile in the lower reaches. Similarly, the SRP concentration in the water is also significantly and positively correlated with the distance from the source. The light availability is also increasing with distance until the shading of the riparian vegetation reaches zero. Overall, the longitudinal gradient of the Holtemme is a characteristic result of the land use progression from relatively undisturbed headwaters to lower reaches shaped by increasing urban and agricultural influence (Wollschläger et al., 2017).

4.2 Shift of biofilm P entrapment from intracellular to extracellular P dominance

Our results show that biofilm P entrapment patterns along the Holtemme are shaped by a shift within the biofilm from a higher share of intracellular P to a higher share of extracellular P of the total P in the biofilm from upper to lower river reaches. These

https://doi.org/10.5194/egusphere-2025-4844
Preprint. Discussion started: 10 October 2025

findings are in line with our first hypothesis. Remarkably, the total P concentration in the biofilm did not change significantly with the increase in available SRP from upper to lower reaches, even though we measured a roughly ten-fold increase of SRP in the water column between the uppermost sampling site and the sampling sites from 21.9 km downwards.

In agreement with our results, Jarvie et al. (2002) found no general increase in total P in biofilm at higher SRP concentrations. However, their study design was a temporal design, and increases in SRP were not necessarily accompanied by changes in the same variables as in our longitudinal design (e.g. light availability). The apparent indifference of the biofilms towards higher SRP loads could be related to legacy P. Since the gradient of SRP along the course of the Holtemme was already shown by previous studies (Weitere et al., 2021), we can assume that especially the biofilms in the lower reaches in our study were well accustomed to relatively high and sustained SRP loads. Taylor et al. (2022) showed that with increasing legacy nutrients, the P accumulation rate of biofilms decreases due to a lower capacity to store additional SRP. This could therefore explain why we found no notable increase in total P in the lower reach biofilms even though SRP loads increased relative to more upstream reaches.

The decreasing share of intracellular P could be explained with active P uptake in upper reach biofilms and a rather passive exchange in lower reach biofilms. Price and Carrick (2016) found in their P addition experiments that biofilms rapidly take up P when the water P concentrations are relatively low, as opposed to when P is added in higher concentrations. They attributed their findings in part to luxury P uptake (P uptake in excess of immediate biological need, Portielje and Lijklema, 1994)), enhanced active P uptake of starved cells, and P uptake saturation through nutrient uptake efficiency loss. This is related to the different uptake mechanisms of P in algae and bacteria outlined by Jansson (1993, 1988). Jansson described a high affinity, active uptake pathway and a low affinity, passive pathway for P intake. The active uptake pathway would assimilate P from outside the cell when the cell is P starved and the P concentration outside the cell is low. Indeed, we found relatively low SRP concentrations at our upstream sampling sites where we also found the highest intracellular P concentrations, which would suggest an active P uptake of the biofilm cells and could hint at the luxury P uptake and storage of P as discussed by Price and Carrick (2016). Further downstream where the intracellular P concentrations were lower and the corresponding SRP concentrations in the water increased, the proportion of extracellular P in the biofilm increased. In ecosystems with relatively low SRP loads, a point source increasing the SRP load can lead to a severe decrease in P uptake efficiency of biofilms (Merseburger et al., 2011). Conditions in the Holtemme river are similar. The lower P uptake efficiency found by Merseburger et al. (2011) could be related to a cessation of active P assimilation in the lower reach biofilms in our study. This is reflected by lower intracellular P concentrations and, at the same time, increased extracellular P concentrations in the EPS through e.g., adsorption of P to the EPS or precipitation of P (Xu et al., 2020). Increased extracellular P at high water SRP concentrations were also found in a single-organism microcosm experiment (Xing et al., 2021). The combined pattern of increasing extracellular P concentrations and decreasing intracellular P concentrations in biofilms with increased P concentrations in the water was also observed in a mesocosm experiment following prolonged exposure to elevated P concentrations (Perujo et al., 2024).

https://doi.org/10.5194/egusphere-2025-4844
Preprint. Discussion started: 10 October 2025

While the discussed findings by other authors show that biofilms exposed long-term to elevated P loads cease active intracellular P entrapment, we expand that by showing that natural biofilm's P entrapment increasingly relies on extracellular P entrapment under these conditions. The EPS seems to act as a natural P buffer, though a saturated intracellular P entrapment capacity counteracts that buffer under sustained high P loads and SRP can reach downstream ecosystems thereby virtually undamped by biofilm activity.

4.3 Potential phosphorus release from sediments increases along the longitudinal river gradient

The potential P release from the sediments, quantified with the EPC_0 method, showed an increase along the longitudinal gradient of the Holtemme river. The uppermost sampling site was considered in equilibrium, while all other sites had a potential for net P release from the sediments. The increase of the EPC_0 from the upstream to downstream sampling sites along the longitudinal gradient of the Holtemme river in light of the increasing concentration of SRP is corroborated by other authors. McDowell (2015) found a strong positive correlation between the EPC_0 and the SRP concentration in a study of 72 lotic water body sites across New Zealand with different geological backgrounds and different land-use intensities. In a meta study, Simpson et al. (2021) showed that this relationship holds true across four orders of magnitude of SRP concentrations and EPC_0 values on a worldwide data set of paired observations of SPR and EPC_0. Though SRP and EPC_0 are positively correlated, this does not necessarily say anything about the actual classification of a sediment as a potential P source or a potential P sink. Simpson et al. (2021) argue that these classifications of sediments as well as the magnitude of EPC_0 and SRP are site specific. An example of this is shown by Ekka et al. (2006). They quantified the EPC_0 before and after WWTPs, which act as strong SRP point sources to streams. The EPC_0 as well as the SRP increased but the classification of the sediment as a potential P source or a P sink did not change due to the higher SRP loads. The change from equilibrium site to potential P source we found in this study could therefore have been caused by other underlying factors.

4.4 Biofilm C metabolic patterns change along the Holtemme

Microbial C metabolic patterns are an expression of microbial functional diversity governed by the DOM pool they are exposed to (Berggren and Del Giorgio, 2015; Ruiz-González et al., 2015). Previous research in the Holtemme River found that bulk DOM lability increased with DOM origin changing from allochthonous dominated DOM to more autochthonous dominated DOM with anthropogenic influences (Kamjunke et al., 2019). Likewise, we found that biofilm C metabolic patterns changed along the river gradient following major land-use changes (Weitere et al., 2021). According to the obtained results on microbial C metabolic patterns, sediment biofilm communities of the Holtemme were divided into three major river sections: the upstream reach with the uppermost sampling site at 6.4 km from the source, the middle reach with the three sampling sites from 12.4 km to 17.4 km and the downstream reach sites with the three sampling sites from 21.9 km to 32.1 km. Freixa et al. (2016), who studied a stream with a comparable pattern of increasing bulk DOM lability as observed in the Holtemme, found their headwater biofilm communities to show functional differences in C use compared to middle reach and downstream biofilms. We found a similar pattern in our upstream site, showing this community to be more specialized in its overall C use

https://doi.org/10.5194/egusphere-2025-4844
Preprint. Discussion started: 10 October 2025

compared to the middle reach biofilm communities which had a higher C use diversity. Moreover, we found the upstream communities to have a lower overall EEA compared to the middle reach communities and – depending on the enzyme in question – the downstream reach communities. This coincides with Freixa et al. (2016) who showed increased middle reach EEAs of BX and BG compared to upstream sites, likely caused by an increase in DOM diversity due to mixing of anthropogenic and natural discharge. Our middle reach biofilm communities were also situated in a more urbanized environment with potential inputs from the surroundings as well as smaller tributaries originating in the Harz mountains. However, data from a sampling campaign in October 2014 by Kamjunke et al. (2019) suggest a reduction in DOM compound diversity in the same river stretch where our middle reach sites are located. Only further downstream, they again detected a higher DOM diversity. The decreased DOM diversity in the middle reaches could explain the higher convergence of C substrate use in our middle reach communities. Our middle reach communities were overall less specialized in their C use, showed a higher C use evenness and very similar patterns between the three sampling sites. The downstream increase in DOM diversity reported by Kamjunke et al. (2019) could be linked to the divergence of substrate use in the lower reach sites we found. This explanation is further corroborated by the findings of Ruiz-González et al. (2015) that bacterial communities in aquatic environments with a higher DOM heterogeneity show a higher functional dissimilarity. This functional dissimilarity among the downstream sites could be related to the WWTP effluent entering the river shortly before the sampling site at 21.9 km. Oest et al. (2018) found biofilm communities downstream of WWTPs to specialize in the degradation of specific anthropogenic compounds. The sampling site furthest downstream shows signs of higher reliance on autochthonously produced DOM. The higher Chl-$a_{sediment}$ and the increasing BX are linked to the degradation of hemicellulose of possibly algal origin. This explanation fits with observations by Freixa and Romaní (2014).

4.5 Linking biofilm C metabolic patterns, biofilm P entrapment patterns and sediment P release patterns

Our hypothesis that a lower C use functional diversity, a lower $ER_{C:P}$ and a lower $Ratio_{Pintra/Pextra}$ would contribute to a higher overall potential P release from the sediment was only partly met. High $ER_{C:N}$ and association with low $ER_{N:P}$ at the uppermost sampling site suggest a high relative microbial investment in the acquisition of C and P (Sinsabaugh et al., 2009) and C-P-co-limitation, as it was described by Pasqualini et al. (2024) for this exact same site. The highest $Ratio_{Pintra/Pextra}$ and intracellular P concentrations found at this site, suggests the apparent P limitation at the uppermost sampling site to be rather an artefact of the continuous active uptake of P discussed above (sect. 4.2). Further, this sampling site showed a high EPS content in the biofilm. EPS, though involved in the uptake of inorganic ions (Flemming and Wingender, 2010) and extracellular P entrapment in particular (Li et al., 2015), was correlated with a high $Ratio_{Pintra/Pextra}$ and by extension low extracellular P contents. Zhou et al. (2017) found in microcosm batch growth experiments with *Synechocystis* sp. that inorganic P was first rapidly adsorbed to the EPS and later taken up into the cells. Furthermore, the concentration of P in the EPS was positively correlated to the protein content in the EPS but not to the carbohydrate content in the study of Zhou et al. (2017). This would suggest that the EPS in the upstream reach can be viewed as a "transient P storage" (Zhang et al., 2013). Moreover, we only measured polysaccharides

https://doi.org/10.5194/egusphere-2025-4844
Preprint. Discussion started: 10 October 2025

(carbohydrates) in the EPS and can't exclude that a low protein content in the EPS could influence the extracellular P entrapment capacity in our biofilms as a whole and in the upstream reach biofilms in particular.

The middle reach biofilms were mainly associated with a high C use functional diversity, the preferential use of different C compounds and a high $ER_{C:P}$, showed neither a relationship to the $Ratio_{Pintra/Pextra}$ nor the P release potential from sediments. From the association with a high $ER_{C:P}$ we can deduce a higher relative investment in the acquisition of C then on P, suggesting a high energy and C demand or a sufficient relative supply of SRP (Moorhead et al., 2023). High $ER_{N:P}$ was connected to the middle reach sites as well, showing a higher relative investment in the acquisition of N over P, and further cementing the conclusion that P demand from organic sources was relatively low (Allison and Vitousek, 2005). The low relative microbial investment into the P procurement from organic sources and the lack of association to the P entrapment variables as well as the EPC_0 show that a high C use functional diversity did not result in a higher biofilm P assimilation. In fact, we showed that biofilms that expressed a high C use functional diversity and were associated with high overall extracellular enzyme expression as well as with a higher relative demand for C and N from organic sources, had a more balanced $Ratio_{Pintra/Pextra}$ compared to the biofilms in our study which were exposed to an environment with less available SRP and lower bulk DOM lability. This could reflect a lower active intracellular P uptake and probably ties into the luxury P uptake idea as well as the finding of Taylor et al. (2022) that legacy P results in lower P accumulation in natural microbial assemblages. When compared to the downstream reach sampling sites, where biofilms had a higher divergence in the overall C use as well as a lower C use functional diversity and higher SRP availability, we found that the middle reach biofilms had an overall higher intracellular P content and higher $Ratio_{Pintra/Pextra}$. This reiterates the unidirectional gradual shift of the P entrapment patterns which is in contrast with the C metabolic patterns which changed more dynamically, showing that microbial communities strongly react to changes in the DOM composition (Ruiz-González et al., 2015).

The downstream reach sites were associated with high SRP values, high DOM bulk lability, high light availability, high Chl-$a_{sediment}$ and high EPC_0. From an extracellular enzyme stoichiometry point of view, these sites were connected to a lower $ER_{C:N}$, showing a higher microbial investment into N acquisition relative to the C acquisition. The increased light availability and the higher Chl-$a_{sediment}$ in the downstream reach could drive the higher relative microbial investment in N acquisition over C acquisition due to an increased algal biomass in the biofilm. Biofilm algal biomass is highly governed by the light availability (Carrick et al., 2023). Moreover, benthic algae and phytoplankton facilitate the expression of extracellular enzymes for the mineralization of N in microbial communities (Rier et al., 2007; Spilling et al., 2023). Romaní and Sabater (2000) showed that a higher share of algal biomass in the biofilm has a positive effect on the extracellular enzyme expression, a relationship we only found to be significant for the APA, though LAP and BX activity were also positively correlated to the Chl-$a_{sediment}$. We didn't find any relationship of the algal biomass to the BG activity, even though this enzyme is generally associated with algal exudates and more labile DOM (Jones and Lock, 1993; Sinsabaugh and Follstad Shah, 2011). Though we didn't find any connection at the downstream reach sites to extracellular enzyme ratios involving P acquiring enzymes, APA was positively correlated with the Chl-$a_{sediment}$ and the EPC_0. This would indicate an involvement of the benthic biofilm community in the P mineralization and possible release of P from the sediments as it was also suggested by Hupfer and Lewandowski (2008). In

https://doi.org/10.5194/egusphere-2025-4844
Preprint. Discussion started: 10 October 2025

fact, several recent studies looked into the possibility of EPC_0 being influenced by sediment microbial activity (DiCarlo et al., 2020; Meyer et al., 2024; Simpson et al., 2020). None of these studies considered the extracellular P adsorbed to the EPS of the biofilms and only Meyer et al. (2024) measured APA but couldn't detect a substantial link between the APA and the EPC_0 due to a generally high APA. Our downstream reach sites were associated with a lower $Ratio_{Pintra/Pextra}$ and by extension with higher extracellular P concentrations. We also found a strong positive correlation between the extracellular P and the EPC_0, further underlining the connection between these two variables. Moreover, APA was positively but not very strongly correlated to the extracellular P. All this evidence suggests a substantial influence of the benthic microbial community on P exchange between the sediments and the water column when the biofilm as a whole – and not only the living cells – is considered.

5 Conclusions

This study addresses the question of intracellular and extracellular P entrapment in biofilms for the first time outside of an experimental setting and connects P entrapment pathways with established methods to assess the whole biofilm metabolism. We showed a shift in the dominance of the biofilm P entrapment pathways along the longitudinal gradient of our studied system and this shift was accompanied by an increase in EPC_0. The contribution of the biofilm C metabolism to the different P entrapment pathways and the EPC_0 seems to be rather unclear on the extremes. A balanced $Ratio_{Pintra/Pextra}$ was connected to a higher C use functional diversity as well as higher EEAs though. The exception was the APA which was related to an increased EPC_0, showing the influence of microbial activity on P-dynamics in the benthic compartment of streams.

P entrapment in biofilms remains an important topic which should be mechanistically explored. The majority of the literature published so far around the different pathways of P entrapment in biofilms (i.e. intracellular and extracellular) focused mostly on the effect of increased P concentrations and P load history in experimental settings. While these are evidently important factors, the role of labile DOM or light availability – the microbial energy sources – on the prevalence of one entrapment pathway over the other are as of yet not individually studied as drivers behind P entrapment pathways. More studies are therefore needed to evaluate the effect of these parameters separately in order to decipher the key mechanisms behind the transition from intracellular to extracellular P entrapment in fluvial biofilms. This study opens up a novel and more holistic view on the P entrapment of benthic biofilms and the P dynamics at the sediment-water interface.

Code and data availability

The data and code are available online upon request at https://doi.org/10.5281/zenodo.17186453

Appendix A: Data table and Spearman's Rank Correlation for predictors

Table A1: Predictor variables at each sampling site. Values are the averages of three replicates at each sampling site, except light availability with five replicates. The standard deviation is in parenthesis. Temperature has no standard deviation since the values were constant for all replicated measurements at each sampling site. The last row shows the distance from the source for each sampling site.

https://doi.org/10.5194/egusphere-2025-4844
Preprint. Discussion started: 10 October 2025

		Site numbers						
Parameters	Units	3	9	11	13	18	22	25
T	°C	12.4	13.5	13.8	14.4	16.0	16.0	16.2
DO	mg L^{-1}	10.19	10.11	10.06	9.88	9.50	9.60	9.70
		(0.01)	(0.02)	(0.02)	(0.02)	(0.00)	(0.01)	(0.02)
pH		6.90	7.91	7.89	7.98	8.01	8.13	8.27
		(0.14)	(0.02	(0.03	(0.01)	(0.01)	(0.01)	(0.01)
Conductivity	µS cm^{-1}	79.63	284.00	300.00	359.00	545.00	591.00	575.67
		(0.12)	(0.00)	(0.00)	(1.00)	(1.00)	(0.00)	(0.58)
DOC	mg L^{-1}	23.87	12.67	12.03	10.83	8.57	6.84	5.96
		(0.72)	(0.15)	(0.06)	(0.47)	(0.18)	(0.50)	(0.18)
NO_3-N	mg L^{-1}	1.17	1.64	1.48	1.55	2.00	2.17	2.16
		(0.01)	(0.02	(0.01)	(0.02)	(0.01)	(0.03)	(0.01)
DNb	mg L^{-1}	2.09	2.25	2.16	2.01	2.75	2.84	2.80
		(0.19)	(0.06)	(0.03)	(0.04)	(0.04)	(0.04)	(0.02)
DP	µg L^{-1}	18.67	18.67	20.33	24.33	121.33	101.00	95.67
		(1.15)	(0.58)	(0.58)	(1.53)	(3.79)	(7.81)	(2.08)
SRP	µg L^{-1}	9.00	13.00	18.33	14.33	110.67	97.00	84.33
		(0.00)	(0.00)	(1.53)	(0.58)	(1.15)	(1.73)	(1.15)
FI		0.95	0.99	1.00	1.02	1.39	1.44	1.35
		(0.01)	(0.01)	(0.00)	(0.02)	(0.03)	(0.01)	(0.03)
BIX		0.34	0.38	0.39	0.41	0.46	0.50	0.52
		(0.01)	(0.01)	(0.00)	(0.01)	(0.01)	(0.01)	(0.01)
Slope Ratio		2.70	2.70	2.97	2.92	3.01	3.50	3.40
		(0.02)	(0.07)	(0.23)	(0.00)	(0.18)	(0.00)	(0.35)
E2:E3		4.57	4.42	4.47	4.49	4.51	4.66	4.64
		(0.01)	(0.02)	(0.02)	(0.01)	(0.03)	(0.05)	(0.06)
Light Availability	% of uncovered sky	17.58 (1.16)	20.32 (7.00)	20.68 (4.26)	38.76 (16.66)	40.98 (10.63)	87.22 (8.15)	100.00 (0.00)
Distance	km	6.4	12.4	16.1	17.4	21.9	27.5	32.1

575

https://doi.org/10.5194/egusphere-2025-4844
Preprint. Discussion started: 10 October 2025

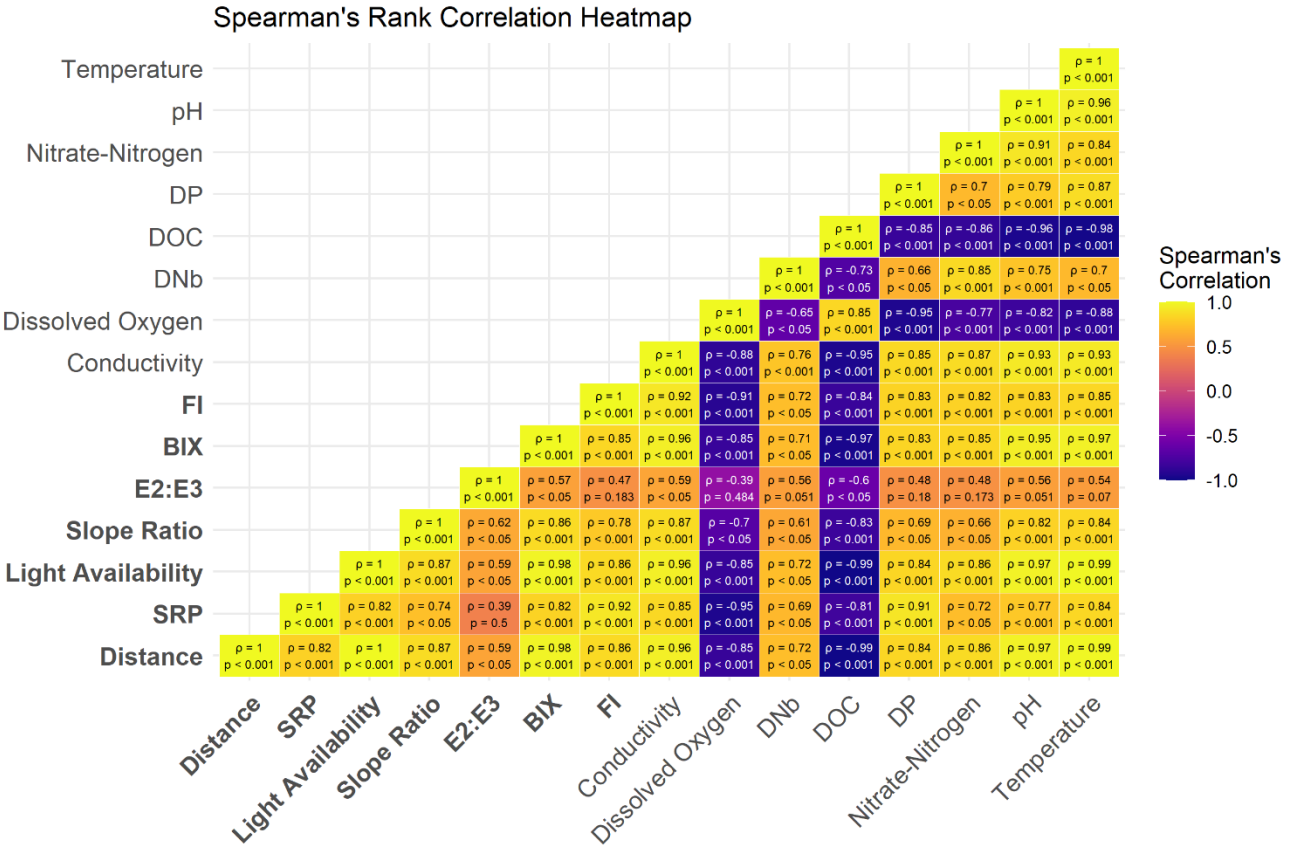

Figure A1: Spearman's rank correlation heatmap showing the correlation of the different predictor variables measured during the longitudinal sampling campaign. ρ-values > 0.7 (or < -0.7 respectively) are considered highly correlated. P-values > 0.05 state a non-statistically significant correlation between the respective predictor variables. P-values are corrected for the type I error inflation through multiple testing with the Benjamin-Yekutieli method. Only the DOM quality proxy E2:E3 was not highly correlated to distance for ρ-values > 0.7 (< -0.7 respectively). The bold variables are the ones shown across the gradient in figure 1 (Fig. 1 A-F).

Appendix B: Results tables for GLMs

Table B1: Accompanying results table for GLMs with a Gamma distribution and log link function analysing the relationship between the P related biofilm variables and the distance from the source (Fig. 2).

Dependent Var.	Independent Var.	Estimate	Std. Error	t-value	p-value
Total P in the biofilm	Distance	0.002	0.009	0.189	0.851
Extracellular P in the biofilm	Distance	0.092	0.016	5.692	< 0.001
Intracellular P in the biofilm	Distance	-0.030	0.018	-1.700	0.101
Ratio P_{intra}/P_{extra}	Distance	-0.132	0.029	-4.617	< 0.001

https://doi.org/10.5194/egusphere-2025-4844
Preprint. Discussion started: 10 October 2025

Table B2: Accompanying results table for GLMs with a Gamma distribution and log link function analysing the relationship between the EPC_0 and the distance from the source (Fig. 3).

Dependent Var.	Independent Var.	Estimate	Std. Error	t-value	p-value
EPC_0	Distance	0.143	0.016	8.895	< 0.001

Table B3: Accompanying results table for GLMs with a Gamma distribution and log link function analysing the relationship between the structural biofilm variables and the distance from the source (Fig. 4 A to C) and zero inflated GLM with a Gamma distribution and log link function analysing the relationship between the Chl-$a_{sediment}$ and the distance from the source (Fig. 4 D).

Dependent Var.	Independent Var.	Estimate	Std. Error	t-value	p-value
AFDW	Distance	-0.002	0.010	-0.165	0.87
EPS	Distance	-0.033	0.009	-3.750	< 0.001
Bacterial Density	Distance	0.016	0.008	1.916	0.064
Dependent Var.	Independent Var.	Estimate	Std. Error	z-value	p-value
Chl-$a_{sediment}$ Gamma part	Distance	0.069	0.010	7.131	< 0.001
Chl-$a_{sediment}$ zero inflated part	Distance	-0.182	0.072	-2.529	< 0.05

Appendix C: Additional analyses for biofilm metabolic profiles

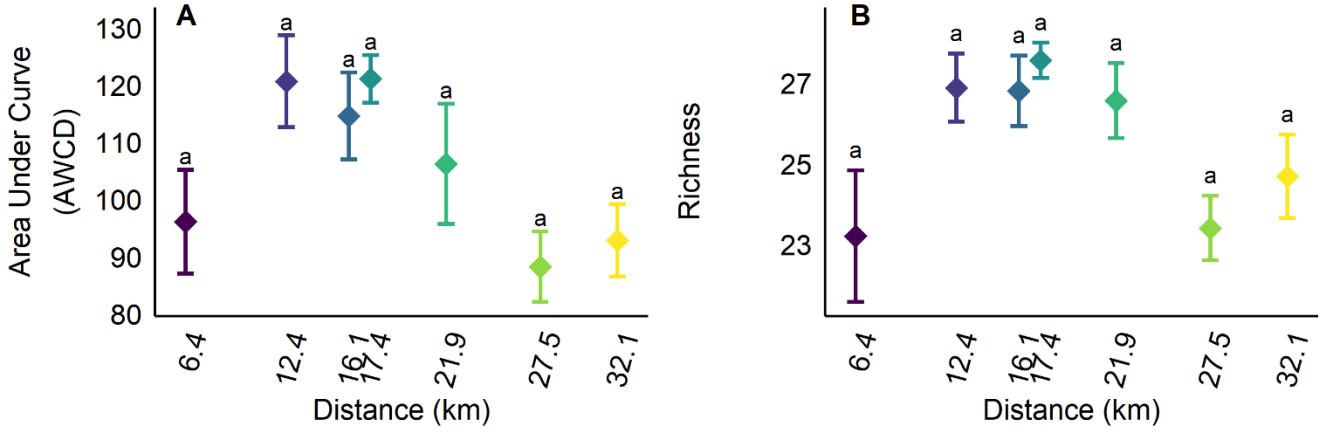

Figure C1: Mean Biolog EcoPlate derived indices for carbon substrate use. Diamonds represent mean values and error bars show the standard error of the mean. Mean values sharing a common letter are not significantly different from each other according to a Tukey's honest significance test at a 5% level of significance. The colours indicate the gradual increase in distance from the source. (A) Area under the curve (AWCD) and (B) substrate richness.

Table C1: One-way ANOVA results table for the differences of the mean Biolog EcoPlate diversity indices (Fig. 5 and Fig. C1). Each model represents one one-way ANOVA.

https://doi.org/10.5194/egusphere-2025-4844
Preprint. Discussion started: 10 October 2025

Model		Df	Sum Sq	Mean Sq	F-statistic	p-value
AWCD	Site	6	5503.744	917.291	3.139	< 0.05
AWCD	Residuals	28	8183.030	292.251		
Shannon Index	Site	6	0.355	0.059	4.826	< 0.05
Shannon Index	Residuals	28	0.343	0.012		
Evenness	Site	6	0.003	0.0006	5.868	< 0.001
Evenness	Residuals	28	0.004	0.0001		
Substrate Richness	Site	6	96.430	16.072	3.261	< 0.05
Substrate Richness	Residuals	28	138.000	4.929		

When we analysed the CLPPs based on the substrate guild use, the repeated measured MANOVA showed significant differences between sites over time (Table C2). The main differences are seen in the canonical variates plot of the CLPPs based on the C substrate guilds (Fig. C2). The first two canonical axes explain 88.05 % of the differences with can1 explaining 58.52 % and can2 explaining 29.53 %. The CLPPs from the sampling sites from 6.4 km to 17.4 km were very similar between them and characterized by their higher ability to use amines and phenolic compounds. The CLPP of the sampling site at 27.5 km was characterized by the high ability to utilize carboxylic acids and polymers, the sampling site furthest downstream was characterized by the ability to degrade carbohydrates and amino acids. The sampling site at 21.9 km showed the highest spread along the x-axis and no direct connection to the potential to utilize any specific substrate guild. ANOVAs for the substrate use for each guild comparing all sampling sites showed significant differences for three of the substrate guilds (Amines, Carbohydrates and Carboxylic Acids). A subsequent Tukey's HSD Test comparing the substrate use for the guilds between sampling sites detected statistical significance only between the sites for the amine use (Fig. C4, Table C4).

Table C2: Type II repeated measures MANOVA for the ilr-coordinates of CLPPs distinguished by substrate guild use. Pillai's Trace test statistic was used. The test revealed significant differences in the substrate guild use incubation time interaction by the different microbial communities. The site effect was non-significant on its own.

Terms	Df	Test Stat	Approx. F	num Df	den Df	p-value
Site	6	.335	2.335	6	28	0.059
Time	1	.593	7.007	5	24	< .001
Site:Time	6	1.324	1.680	30	140	0.024

https://doi.org/10.5194/egusphere-2025-4844
Preprint. Discussion started: 10 October 2025

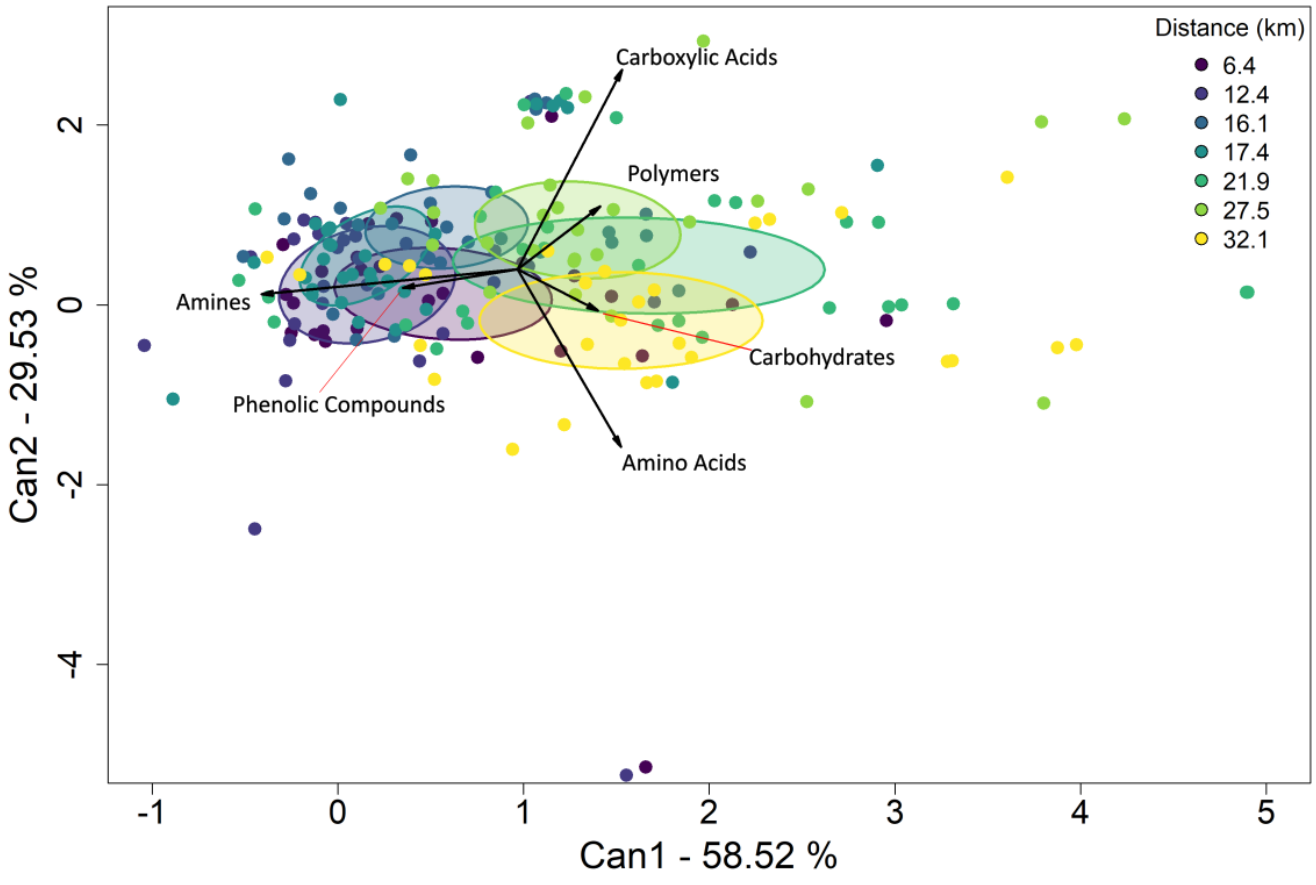

Figure C2: Canonical variates plot of the CLPPs derived from compositional data of the Biolog EcoPlates absorbance data for each guild. The data points are coloured according to the sampling site and the distance from the source of the stream. The ellipses group the majority of the samples for each site.

The repeated measures MANOVA testing for differences in the interaction of the sampling site and the incubation time did not show a significant difference between the CLPPs (Table C3), major patterns could be identified though (Fig. C3). These patterns show a clear distinction between sampling sites by Biolog EcoPlate substrate use. The sampling site at 6.4 km was distinguished by a higher use of D-Mannose (D.Mann), the sampling sites from 12.4 km to 17.4 km were distinguished by a preferential use of D-Cellobiose (D.Cell), Pyruvic acid methyl ester (PAME) and Putrescine (Putr). The microbial community of the sampling site at 21.9 km preferentially used the compounds D-Malic acid (D.MalA) and Tween 40 (Tw40). A preferential use for Tween 80 (Tw80) and N-Acetyl-D-glucosamine (N.A.D.Gluc) was found for the microbial communities from the sampling site at 27.5 km. The most downstream sampling site at 32.1 km was in the center of the plot with a preferential use of Glycogen (Glyc), L-Serine (L.Ser) and D-Galactonic acid c-lactone (D.G.Lact).

Table C3: Type II repeated measures MANOVA for the ilr-coordinates of CLPPs distinguished by Biolog Ecoplate carbon substrates use. Pillai's Trace test statistic was used. The test revealed no significant differences in the substrate-use-incubation-time-interaction by the different microbial communities.

https://doi.org/10.5194/egusphere-2025-4844
Preprint. Discussion started: 10 October 2025

Terms	Df	Test Stat	Approx. F	num Df	den Df	p-value
Site	6	.080	.41	6	28	0.760
Time	1	.440	4.92	4	25	< .05
Site:Time	6	.989	1.53	24	112	0.143

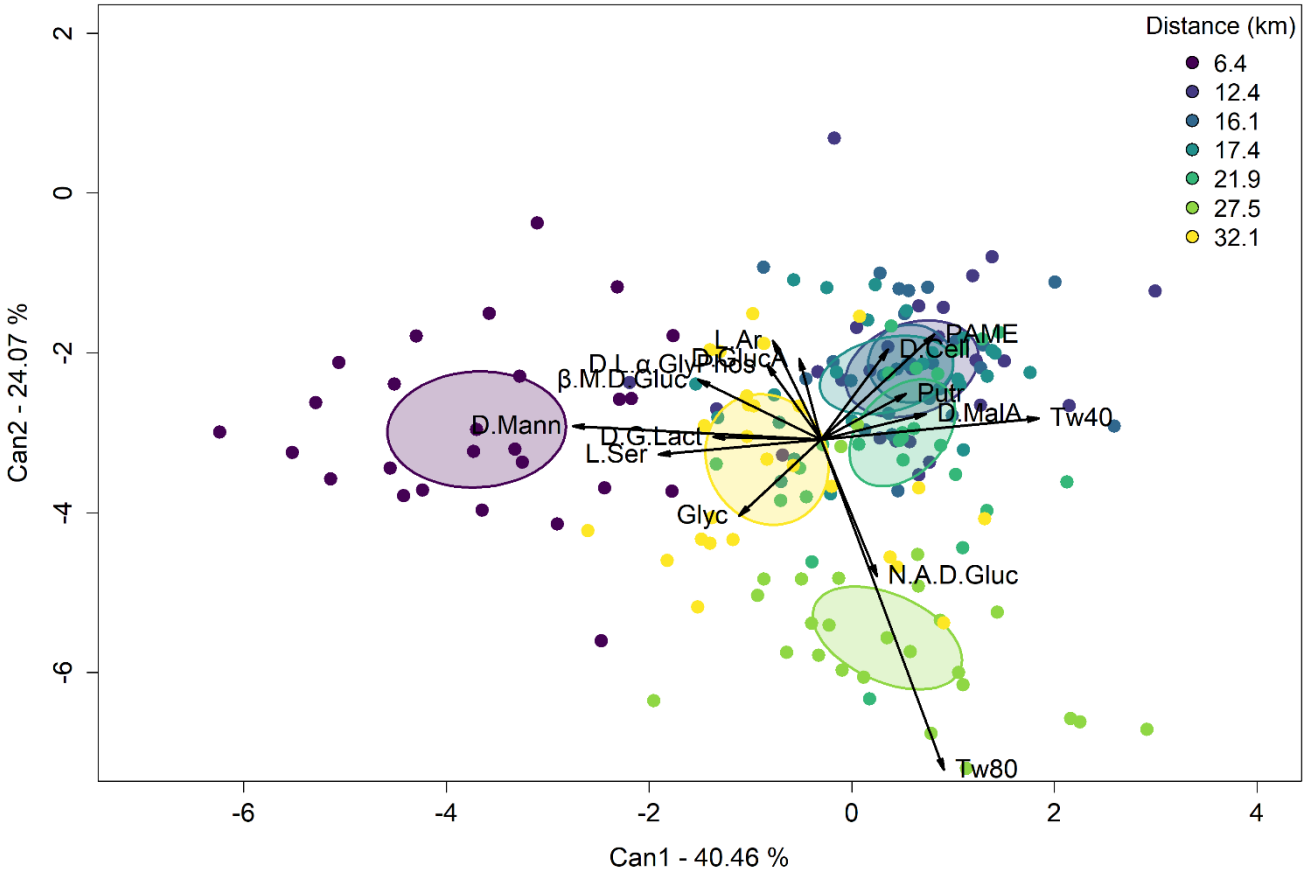

635 **Figure C3: Canonical variates plot of the CLPPs derived from compositional data of the Biolog EcoPlates absorbance data for each carbon substrate. The data points are coloured according to the sampling site and the distance from the source of the stream. The ellipses group the majority of the samples for each site.**

https://doi.org/10.5194/egusphere-2025-4844
Preprint. Discussion started: 10 October 2025

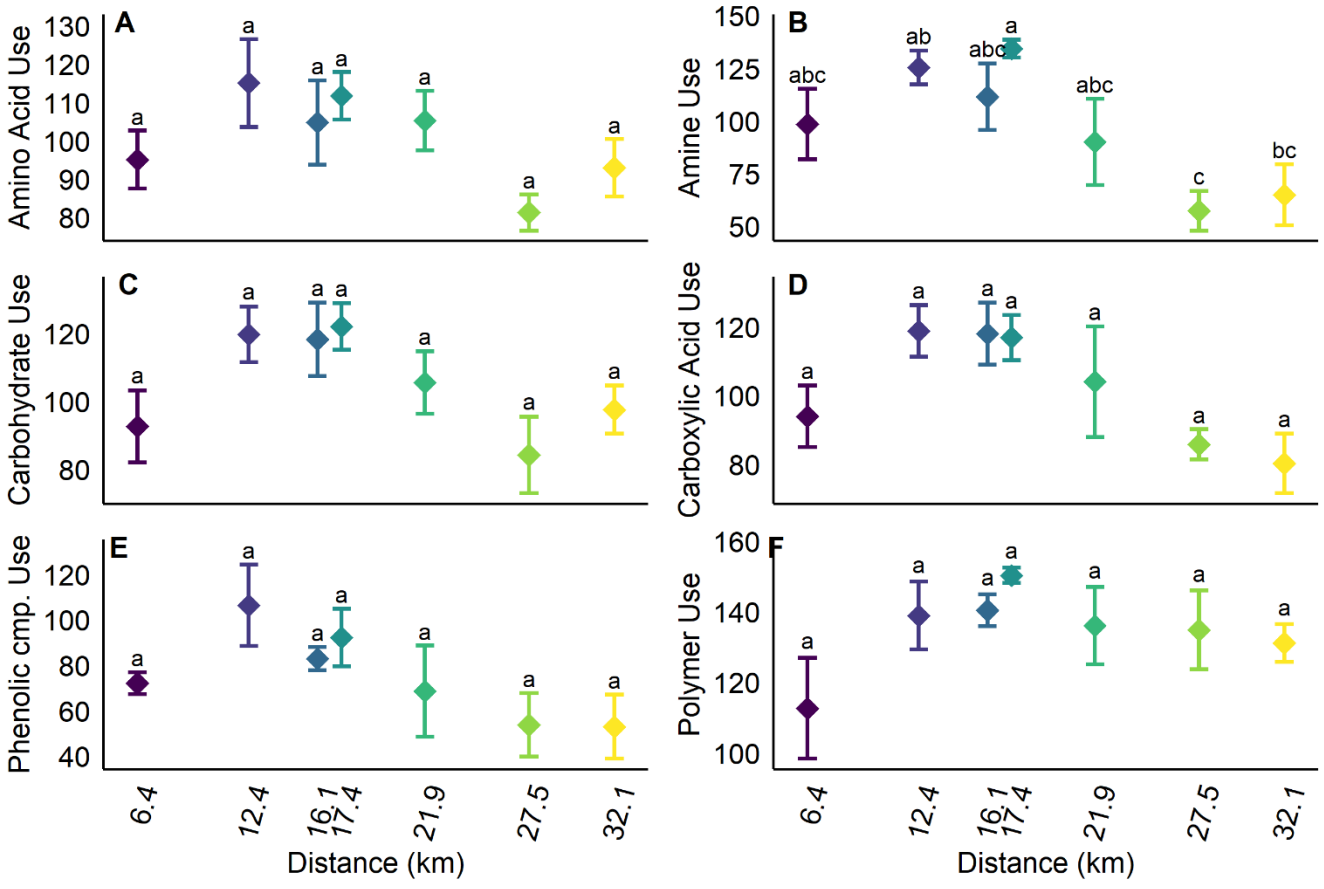

Figure C4: Biolog EcoPlate substrate use divided into substrate guilds as the AUC (AWCD) of each substrate guild. Diamonds represent mean values and error bars show the standard error of the mean. Mean values sharing a common letter are not significantly different from each other according to a Tukey's honest significance test at a 5% level of significance. The colours indicate the gradual increase in distance from the source. (A) Amino Acid Use, (B) Amine Use, (C) Carbohydrate Use, (D) Carboxylic Acid Use, (E) Phenolic Compound Use and (F) Polymer Use.

Table C4: One-way ANOVA results table for the differences of the Biolog EcoPlate substrate use divided into substrate guilds as the mean AUC of each substrate guild (Fig. S 5). Each model represents one one-way ANOVA.

Model		Df	Sum Sq	Mean Sq	F-statistic	p-value
Amino Acid Use	Site	6	4167.84	694.64	1.99	0.100
Amino Acid Use	Residuals	28	9760.31	348.58		
Amine Use	Site	6	25262.57	4210.43	4.43	0.003
Amine Use	Residuals	28	26606.13	950.22		
Carbohydrate Use	Site	6	6582.82	1097.14	2.55	0.043
Carbohydrate Use	Residuals	28	12054.51	430.52		
Carboxylic Acid Use	Site	6	7824.87	1304.15	2.96	0.023

https://doi.org/10.5194/egusphere-2025-4844
Preprint. Discussion started: 10 October 2025

Carboxylic Acid Use	Residuals	28	12326.54	440.23		
Phenolic Compound Use	Site	6	11604.65	1934.11	2.05	0.092
Phenolic Compound Use	Residuals	28	26418.68	943.52		
Polymer Use	Site	6	3981.40	663.57	1.56	0.195
Polymer Use	Residuals	28	11886.92	424.53		

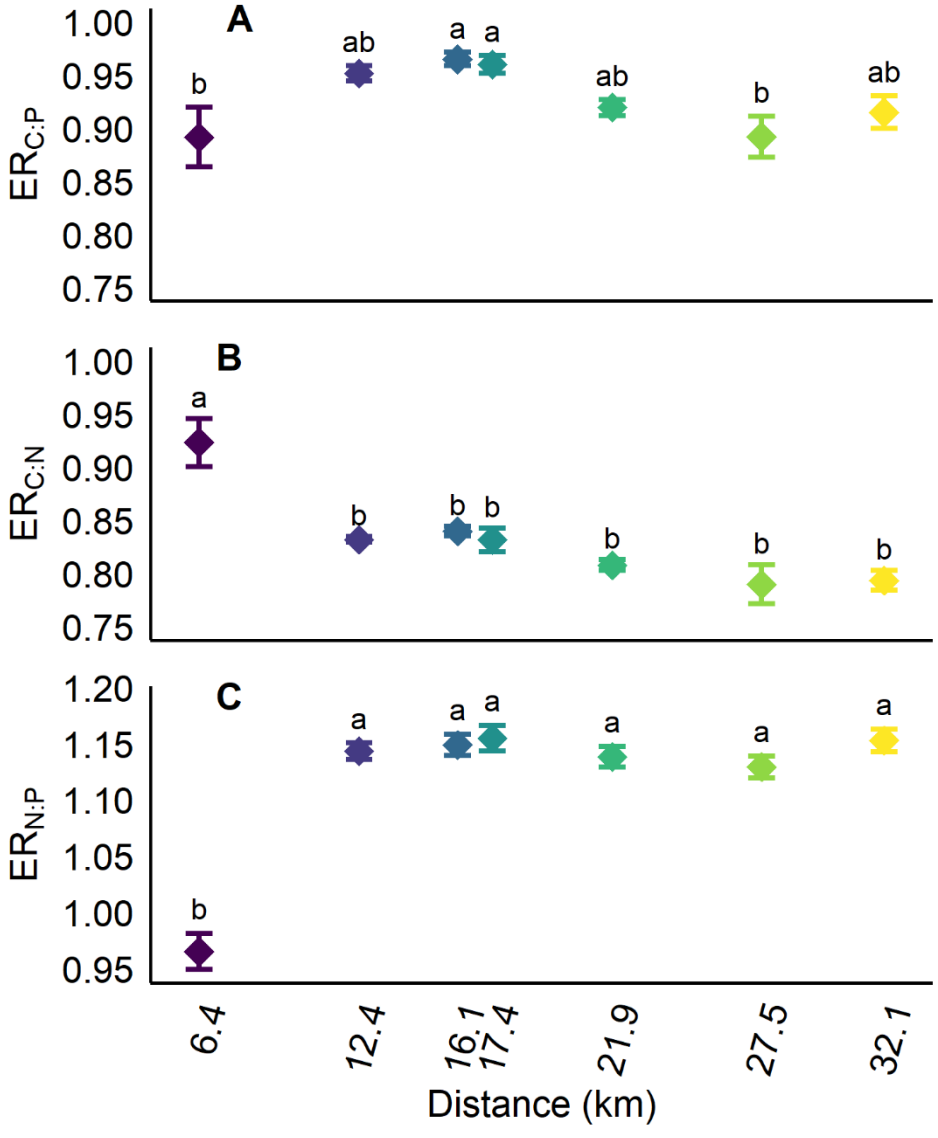

Figure C5: Stoichiometric ratios of extracellular enzymatic activities. Diamonds represent mean values and error bars show the standard error of the mean. Mean values sharing a common letter are not significantly different from each other according to a Tukey's honest significance test at a 5% level of significance. The colours indicate the gradual increase in distance from the source.

https://doi.org/10.5194/egusphere-2025-4844
Preprint. Discussion started: 10 October 2025

(A) $ER_{C:P}$ (logarithmic ratios of measured C and P acquiring extracellular enzymes), (B) $ER_{C:N}$ (logarithmic ratios of measured C and N acquiring extracellular enzymes) and (C) $ER_{N:P}$ (logarithmic ratios of measured N and P acquiring extracellular enzymes).

The mean $ER_{C:P}$ was slightly below 1 with values ranging from 0.89 to 0.96. Specifically, the most upstream site showed the lowest value together with the three most downstream sites from 21.9 km to 32.1 km. The middle reach sites from 12.4 km to 17.4 km showed the highest mean $ER_{C:P}$ and had significantly higher $ER_{C:P}$ than the uppermost sampling site and the sampling site at 27.5 km ($p < 0.05$, Fig. C5 A, Table C5).

For the $ER_{C:N}$, the ANOVA with subsequent Tukey's HSD test revealed a significantly higher ratio for the uppermost sampling site compared to all the other sites ($p < 0.001$), which didn't statistically differ between each other. The mean $ER_{C:N}$ for the uppermost site was 0.92 and therefore relatively balanced while the $ER_{C:N}$ for the other sites ranged from 0.84 (sampling site at 16.4 km) to 0.79 at two most downstream sampling sites (Fig. C5 B, Table C5).

The mean $ER_{N:P}$ ranged from 0.97 at the uppermost sampling site to 1.16 at the sampling site at 17.4 km. At the most downstream sampling site the $ER_{N:P}$ was at 1.15. The $ER_{N:P}$ of the uppermost sampling site was significantly lower compared to all other sites ($p < 0.001$, Fig C5 C, Table C5).

Table C5: One-way ANOVA results table for the differences of the mean extracellular enzyme activities and extracellular enzymatic ratios between sites (Fig. C5). Each model represents one one-way ANOVA.

Model		Df	Sum Sq	Mean Sq	F-statistic	p-value
Phosphatase	Site	6	54516.59	9086.10	298.30	< 0.001
Phosphatase	Residuals	28	852.88	30.46		
Leucine Aminopeptidase	Site	6	1040442.66	173407.11	28.08	< 0.001
Leucine Aminopeptidase	Residuals	28	173034.70	6179.81		
β-Glucosidase	Site	6	25392.44	4232.07	13.73	< 0.001
β-Glucosidase	Residuals	28	8633.23	308.33		
β-Xylosidase	Site	6	12301.36	2050.23	11.84	< 0.001
β-Xylosidase	Residuals	28	4847.29	173.12		
$ER_{C:P}$	Site	6	0.03	0.005	4.20	< 0.05
$ER_{C:P}$	Residuals	28	0.03	0.001		
$ER_{C:N}$	Site	6	0.06	0.0102	12.77	< 0.001
$ER_{C:N}$	Residuals	28	0.02	0.0008		
$ER_{N:P}$	Site	6	0.14	0.0234	40.80	< 0.001
$ER_{N:P}$	Residuals	28	0.02	0.0006		

https://doi.org/10.5194/egusphere-2025-4844
Preprint. Discussion started: 10 October 2025

Appendix D: Spearman's Rank Correlation for variables used in the PCA (Fig. 7)

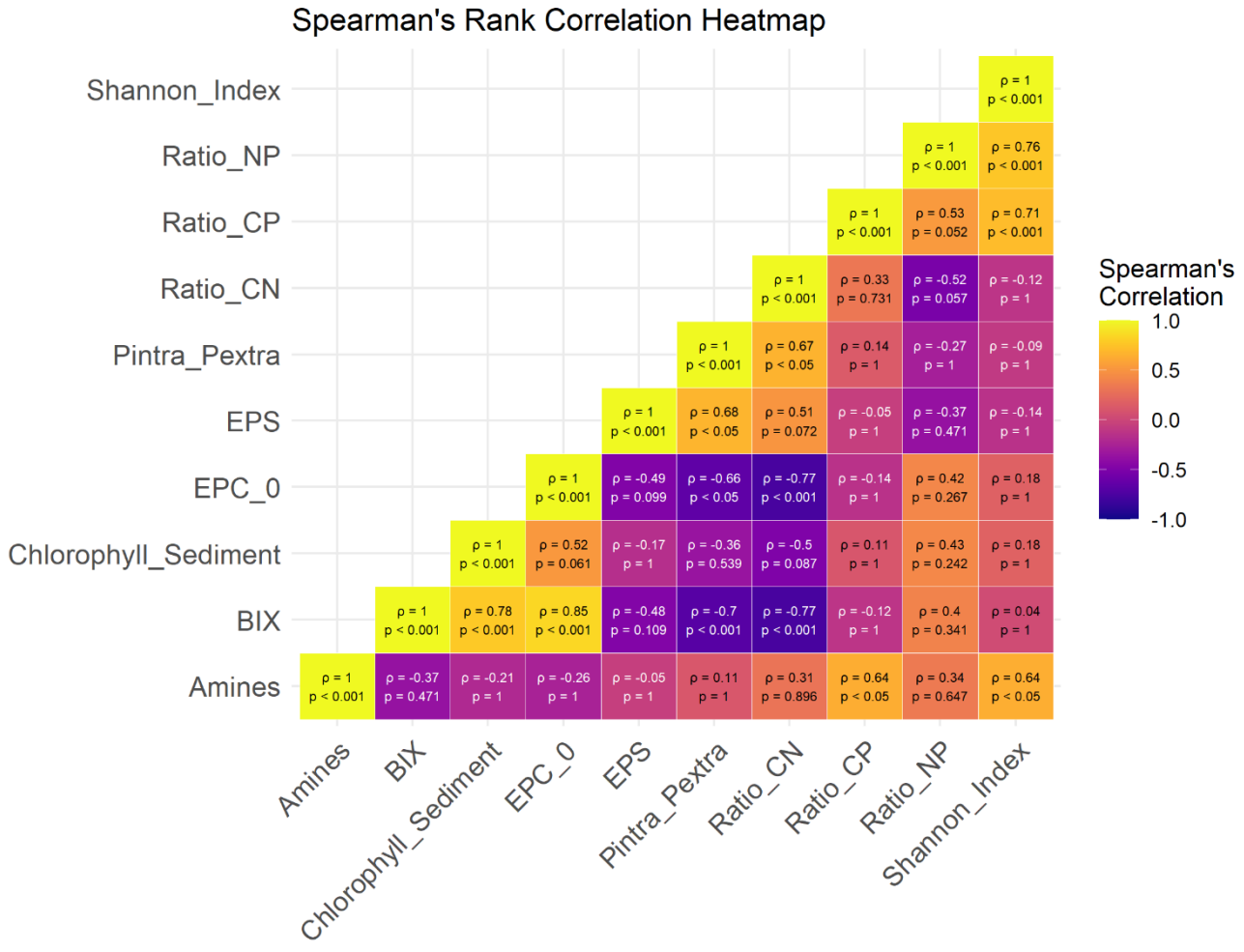

Figure D1: Spearman's rank correlation heatmap showing the correlation of the different variables used in the PCA (Fig. 7). ρ-values > 0.7 (or < -0.7 respectively) are considered highly correlated. P-values > 0.05 state a non-statistically significant correlation between the respective predictor variables. P-values are corrected for the type I error inflation through multiple testing with the Benjamin-Yekutieli method.

Author contributions

All authors were part of the conceptualization. Data curation and formal analysis was done by SW. Funding acquisition was done by NP and MW. Methodology was developed by NP and executed by NP and SW. The administration of the project was done by SW. SW was supervised by all co-authors. Visualization of the data was done by SW. Writing of the first draft was done by SW, all authors were involved in the review and editing of the manuscript.

https://doi.org/10.5194/egusphere-2025-4844
Preprint. Discussion started: 10 October 2025

Competing interests

The authors declare that they have no conflict of interest.

Acknowledgements

We wish to thank Luisa Weber for her help during the field campaign. Special thanks go out to Andrea Hoff, Anne Ballmann, Ina Siebert, Kerstin Lerche and Nils Ribbe for their support in the laboratory analyses. Furthermore, we sincerely thank Ulrike Schlägel for her contribution to the statistical analyses of the data. This research was funded by the German Research Foundation (DFG) as part of the FLUPHOS project (project number 514547471). AI tools, namely ChatGPT, were used for the translation of specific words from German to English as well as to find synonyms and check for the grammatical correctness of certain sentences.

References:

Allison, S.D., Vitousek, P.M., 2005. Responses of extracellular enzymes to simple and complex nutrient inputs. Soil Biol. Biochem. 37, 937–944. https://doi.org/10.1016/j.soilbio.2004.09.014

Amalfitano, S., Puddu, S.F., Alberto, 2009. Flow cytometric analysis of benthic prokaryotes attached to sediment particles. J. Microbiol. Methods 79, 246–249. https://doi.org/10.1016/j.mimet.2009.09.005

Battin, T.J., Besemer, K., Bengtsson, M.M., Romani, A.M., Packmann, A.I., 2016. The ecology and biogeochemistry of stream biofilms. Nat. Rev. Microbiol. 14, 251–263. https://doi.org/10.1038/nrmicro.2016.15

Benjamini, Y., Yekutieli, D., 2001. The control of the false discovery rate in multiple testing under dependency. Ann. Stat. 29. https://doi.org/10.1214/aos/1013699998

Berggren, M., Del Giorgio, P.A., 2015. Distinct patterns of microbial metabolism associated to riverine dissolved organic carbon of different source and quality. J. Geophys. Res. Biogeosciences 120, 989–999. https://doi.org/10.1002/2015JG002963

Carrick, H.J., Marble, C., Tian, Y.Q., 2023. Differential responses for stream algal assemblages exposed to factorial N and P enrichment along an in situ DOC gradient. Front. Environ. Sci. 11, 1066586. https://doi.org/10.3389/fenvs.2023.1066586

Chianucci, F., Puletti, N., Ferrara, C., 2023. coveR2: Process Digital Cover Photography Images of Tree Crowns. https://doi.org/10.32614/CRAN.package.coveR2

https://doi.org/10.5194/egusphere-2025-4844
Preprint. Discussion started: 10 October 2025

Correll, D., 1999. Phosphorus: a rate limiting nutrient in surface waters. Poult. Sci. 78, 674–682. https://doi.org/10.1093/ps/78.5.674

Cory, R.M., McKnight, D.M., 2005. Fluorescence Spectroscopy Reveals Ubiquitous Presence of Oxidized and Reduced Quinones in Dissolved Organic Matter. Environ. Sci. Technol. 39, 8142–8149. https://doi.org/10.1021/es0506962

DiCarlo, A.M., Weisener, Chris.G., Drouillard, Ken.G., 2020. Evidence for Microbial Community Effect on Sediment Equilibrium Phosphorus Concentration (EPC0). Bull. Environ. Contam. Toxicol. 105, 736–741. https://doi.org/10.1007/s00128-020-03019-0

Dodds, W., Smith, V., 2016. Nitrogen, phosphorus, and eutrophication in streams. Inland Waters 6, 155–164. https://doi.org/10.5268/iw-6.2.909

DuBois, Michel., Gilles, K.A., Hamilton, J.K., Rebers, P.A., Smith, Fred., 1956. Colorimetric Method for Determination of Sugars and Related Substances. Anal. Chem. 28, 350–356. https://doi.org/10.1021/ac60111a017

Duhamel, S., 2024. The microbial phosphorus cycle in aquatic ecosystems. Nat. Rev. Microbiol. https://doi.org/10.1038/s41579-024-01119-w

Ekka, S.A., Haggard, B.E., Matlock, M.D., Chaubey, I., 2006. Dissolved phosphorus concentrations and sediment interactions in effluent–dominated Ozark streams. Ecol. Eng. 26, 375–391. https://doi.org/10.1016/j.ecoleng.2006.01.002

Fischer, H., 2003. The Role of Biofilms in the Uptake and Transformation of Dissolved Organic Matter, in: Aquatic Ecosystems. Elsevier, pp. 285–313. https://doi.org/10.1016/B978-012256371-3/50013-5

Flemming, H.-C., Wingender, J., 2010. The biofilm matrix. Nat. Rev. Microbiol. 8, 623–633. https://doi.org/10.1038/nrmicro2415

Freixa, A., Ejarque, E., Crognale, S., Amalfitano, S., Fazi, S., Butturini, A., Romaní, A.M., 2016. Sediment microbial communities rely on different dissolved organic matter sources along a Mediterranean river continuum. Limnol. Oceanogr. 61, 1389–1405. https://doi.org/10.1002/lno.10308

Freixa, A., Romaní, A.M., 2014. Shifts in carbon substrate utilization in sediment microbial communities along the Llobregat River. Fundam. Appl. Limnol. 185, 247–261. https://doi.org/10.1127/fal/2014/0588

Freixa Casals, A., 2016. Function and structure of river sediment biofilms and their role in organic matter utilization. Universitat de Girona, Girona.

https://doi.org/10.5194/egusphere-2025-4844
Preprint. Discussion started: 10 October 2025

Garland, J.L., Mills, A.L., 1991. Classification and Characterization of Heterotrophic Microbial Communities on the Basis of Patterns of Community-Level Sole-Carbon-Source Utilization. Appl. Environ. Microbiol. 57, 2351–2359. https://doi.org/10.1128/aem.57.8.2351-2359.1991

Guckert, J.B., Carr, G.J., Johnson, T.D., Hamm, B.G., Davidson, D.H., Kumagai, Y., 1996. Community analysis by Biolog: curve integration for statistical analysis of activated sludge microbial habitats. J. Microbiol. Methods 27, 183–197. https://doi.org/10.1016/S0167-7012(96)00948-7

Helms, J.R., Stubbins, A., Ritchie, J.D., Minor, E.C., Kieber, D.J., Mopper, K., 2008. Absorption spectral slopes and slope ratios as indicators of molecular weight, source, and photobleaching of chromophoric dissolved organic matter. Limnol. Oceanogr. 53, 955–969. https://doi.org/10.4319/lo.2008.53.3.0955

Huguet, A., Vacher, L., Relexans, S., Saubusse, S., Froidefond, J.M., Parlanti, E., 2009. Properties of fluorescent dissolved organic matter in the Gironde Estuary. Org. Geochem. 40, 706–719. https://doi.org/10.1016/j.orggeochem.2009.03.002

Hupfer, M., Lewandowski, J., 2008. Oxygen Controls the Phosphorus Release from Lake Sediments – a Long-Lasting Paradigm in Limnology. Int. Rev. Hydrobiol. 93, 415–432. https://doi.org/10.1002/iroh.200711054

Inamdar, S., Sienkiewicz, N., Lutgen, A., Jiang, G., Kan, J., 2020. Streambank Legacy Sediments in Surface Waters: Phosphorus Sources or Sinks? Soil Syst. 4, 30. https://doi.org/10.3390/soilsystems4020030

Jansson, M., 1993. Uptake, exchange and excretion of orthophosphate in phosphate-starved Scenedesmus quadricauda and Pseudomonas K7. Limnol. Oceanogr. 38, 1162–1178. https://doi.org/10.4319/lo.1993.38.6.1162

Jansson, M., 1988. Phosphate uptake and utilization by bacteria and algae. Hydrobiologia 170, 177–189. https://doi.org/10.1007/BF00024904

Jarvie, H.P., Jürgens, M.D., Williams, R.J., Neal, C., Davies, J.J.L., Barrett, C., White, J., 2005. Role of river bed sediments as sources and sinks of phosphorus across two major eutrophic UK river basins: the Hampshire Avon and Herefordshire Wye. J. Hydrol. 304, 51–74. https://doi.org/10.1016/j.jhydrol.2004.10.002

Jarvie, H.P., Neal, C., Warwick, A., White, J., Neal, M., Wickham, H.D., Hill, L.K., Andrews, M.C., 2002. Phosphorus uptake into algal biofilms in a lowland chalk river. Sci. Total Environ. 282–283, 353–373. https://doi.org/10.1016/S0048-9697(01)00924-X

Jones, S.E., Lock, M.A., 1993. Seasonal determinations of extracellular hydrolytic activities in heterotrophic and mixed heterotrophic/autotrophic biofilms from two contrasting rivers. Hydrobiologia 257, 1–16. https://doi.org/10.1007/BF00013991

https://doi.org/10.5194/egusphere-2025-4844
Preprint. Discussion started: 10 October 2025

Kamjunke, N., Hertkorn, N., Harir, M., Schmitt-Kopplin, P., Griebler, C., Brauns, M., Von Tümpling, W., Weitere, M., Herzsprung, P., 2019. Molecular change of dissolved organic matter and patterns of bacterial activity in a stream along a land-use gradient. Water Res. 164, 114919. https://doi.org/10.1016/j.watres.2019.114919

Li, W.-W., Zhang, H.-L., Sheng, G.-P., Yu, H.-Q., 2015. Roles of extracellular polymeric substances in enhanced biological phosphorus removal process. Water Res. 86, 85–95. https://doi.org/10.1016/j.watres.2015.06.034

Lock, M.A., Wallace, R.R., Costerton, J.W., Ventullo, R.M., Charlton, S.E., 1984. River Epilithon: Toward a Structural-Functional Model. Oikos 42, 10. https://doi.org/10.2307/3544604

Mainstone, C.P., Parr, W., 2002. Phosphorus in rivers — ecology and management. Sci. Total Environ. 282–283, 25–47. https://doi.org/10.1016/S0048-9697(01)00937-8

McDowell, R.W., 2015. Relationship between Sediment Chemistry, Equilibrium Phosphorus Concentrations, and Phosphorus Concentrations at Baseflow in Rivers of the New Zealand National River Water Quality Network. J. Environ. Qual. 44, 921–929. https://doi.org/10.2134/jeq2014.08.0362

Merseburger, G., Martí, E., Sabater, F., Ortiz, J.D., 2011. Point-source effects on N and P uptake in a forested and an agricultural Mediterranean streams. Sci. Total Environ. 409, 957–967. https://doi.org/10.1016/j.scitotenv.2010.11.014

Meyer, M., Koschorreck, M., Weitere, M., Kneis, D., Perujo, N., 2024. Dissolved organic matter quality, hydrological connectivity and microbial activity shape phosphorus buffering in river-floodplain systems. Sci. Total Environ. 957, 177452. https://doi.org/10.1016/j.scitotenv.2024.177452

Minero, C., Lauri, V., Falletti, G., Maurino, V., Pelizzetti, E., Vione, D., 2007. Spectrophotometric Characterisation of Surface Lakewater Samples: Implications for the Quantification of Nitrate and the Properties of Dissolved Organic Matter. Ann. Chim. 97, 1107–1116. https://doi.org/10.1002/adic.200790094

Moorhead, D., Cui, Y., Sinsabaugh, R., Schimel, J., 2023. Interpreting patterns of ecoenzymatic stoichiometry. Soil Biol. Biochem. 180, 108997. https://doi.org/10.1016/j.soilbio.2023.108997

Oest, A., Alsaffar, A., Fenner, M., Azzopardi, D., Tiquia-Arashiro, S.M., 2018. Patterns of Change in Metabolic Capabilities of Sediment Microbial Communities in River and Lake Ecosystems. Int. J. Microbiol. 2018, 1–15. https://doi.org/10.1155/2018/6234931

https://doi.org/10.5194/egusphere-2025-4844
Preprint. Discussion started: 10 October 2025

Oviedo-Vargas, D., Royer, T.V., Johnson, L.T., 2013. Dissolved organic carbon manipulation reveals coupled cycling of carbon, nitrogen, and phosphorus in a nitrogen-rich stream. Limnol. Oceanogr. 58, 1196–1206. https://doi.org/10.4319/lo.2013.58.4.1196

Pasqualini, J., Graeber, D., Bartusch, A., Kümmel, S., Hernandez, Z.L.D., Musat, N., Sunjidmaa, N., Weitere, M., Brauns, M., 2024. Disentangling effects of multiple agricultural stressors on benthic and hyporheic nitrate uptake. Biogeochemistry 167, 287–299. https://doi.org/10.1007/s10533-024-01130-6

Perujo, N., Freixa, A., Vivas, Z., Gallegos, A.M., Butturini, A., Romaní, A.M., 2016. Fluvial biofilms from upper and lower river reaches respond differently to wastewater treatment plant inputs. Hydrobiologia 765, 169–183. https://doi.org/10.1007/s10750-015-2411-1

Perujo, N., Graeber, D., Fink, P., Neuert, L., Sunjidmaa, N., Weitere, M., 2025. Bioavailable Dissolved Organic Carbon Serves as a Key Regulator of Phosphorus Dynamics in Stream Biofilms. Environ. Microbiol. Rep. 17, e70115. https://doi.org/10.1111/1758-2229.70115

Perujo, N., Neuert, L., Fink, P., Weitere, M., 2024. Saturation of intracellular phosphorus uptake and prevalence of extracellular phosphorus entrapment in fluvial biofilms after long-term P pulses: Implications for river self-purification. Sci. Total Environ. 952, 175976. https://doi.org/10.1016/j.scitotenv.2024.175976

Perujo, N., Romaní, A.M., Martín-Fernández, J.A., 2020. Microbial community-level physiological profiles: Considering whole data set and integrating dynamics of colour development. Ecol. Indic. 117, 106628. https://doi.org/10.1016/j.ecolind.2020.106628

Perujo, N., Sanchez-Vila, X., Proia, L., Romaní, A.M., 2017. Interaction between Physical Heterogeneity and Microbial Processes in Subsurface Sediments: A Laboratory-Scale Column Experiment. Environ. Sci. Technol. 51, 6110–6119. https://doi.org/10.1021/acs.est.6b06506

Portielje, R., Lijklema, L., 1994. Kinetics of luxury uptake of phosphate by algae-dominated benthic communities. Hydrobiologia 275–276, 349–358. https://doi.org/10.1007/BF00026725

Price, K.J., Carrick, H.J., 2016. Effects of experimental nutrient loading on phosphorus uptake by biofilms: evidence for nutrient saturation in mid-Atlantic streams. Freshw. Sci. 35, 503–517. https://doi.org/10.1086/686269

R Core Team, 2021. R: A language and environment for statistical computing.

https://doi.org/10.5194/egusphere-2025-4844
Preprint. Discussion started: 10 October 2025

Rier, S.T., Kuehn, K.A., Francoeur, S.N., 2007. Algal regulation of extracellular enzyme activity in stream microbial communities associated with inert substrata and detritus. J. North Am. Benthol. Soc. 26, 439–449. https://doi.org/10.1899/06-080.1

Roberts, E.J., Cooper, R.J., 2018. Riverbed sediments buffer phosphorus concentrations downstream of sewage treatment works across the River Wensum catchment, UK. J. Soils Sediments 18, 2107–2116. https://doi.org/10.1007/s11368-018-1939-x

Romaní, A.M., Giorgi, A., Acuña, V., Sabater, S., 2004. The influence of substratum type and nutrient supply on biofilm organic matter utilization in streams. Limnol. Oceanogr. 49, 1713–1721. https://doi.org/10.4319/lo.2004.49.5.1713

Romaní, A.M., Sabater, S., 2001. STRUCTURE AND ACTIVITY OF ROCK AND SAND BIOFILMS IN A MEDITERRANEAN STREAM. Ecology 82, 3232–3245. https://doi.org/10.1890/0012-9658(2001)082[3232:SAAORA]2.0.CO;2

Romaní, A.M., Sabater, S., 2000. Influence of Algal Biomass on Extracellular Enzyme Activity in River Biofilms. Microb. Ecol. 40, 16–24. https://doi.org/10.1007/s002480000041

Ruiz-González, C., Niño-García, J.P., Lapierre, J., Del Giorgio, P.A., 2015. The quality of organic matter shapes the functional biogeography of bacterioplankton across boreal freshwater ecosystems. Glob. Ecol. Biogeogr. 24, 1487–1498. https://doi.org/10.1111/geb.12356

Simpson, Z.P., McDowell, R.W., Condron, L.M., 2020. The biotic contribution to the benthic stream sediment phosphorus buffer. Biogeochemistry 151, 63–79. https://doi.org/10.1007/s10533-020-00709-z

Simpson, Z.P., McDowell, R.W., Condron, L.M., 2019. The error in stream sediment phosphorus fractionation and sorption properties effected by drying pretreatments. J. Soils Sediments 19, 1587–1597. https://doi.org/10.1007/s11368-018-2180-3

Simpson, Z.P., McDowell, R.W., Condron, L.M., McDaniel, M.D., Jarvie, H.P., Abell, J.M., 2021. Sediment phosphorus buffering in streams at baseflow: A meta-analysis. J. Environ. Qual. 50, 287–311. https://doi.org/10.1002/jeq2.20202

Sinsabaugh, R.L., Follstad Shah, J.J., 2011. Ecoenzymatic stoichiometry of recalcitrant organic matter decomposition: the growth rate hypothesis in reverse. Biogeochemistry 102, 31–43. https://doi.org/10.1007/s10533-010-9482-x

Sinsabaugh, R.L., Hill, B.H., Follstad Shah, J.J., 2009. Ecoenzymatic stoichiometry of microbial organic nutrient acquisition in soil and sediment. Nature 462, 795–798. https://doi.org/10.1038/nature08632

https://doi.org/10.5194/egusphere-2025-4844
Preprint. Discussion started: 10 October 2025

Sinsabaugh, R.L., Lauber, C.L., Weintraub, M.N., Ahmed, B., Allison, S.D., Crenshaw, C., Contosta, A.R., Cusack, D., Frey, S., Gallo, M.E., Gartner, T.B., Hobbie, S.E., Holland, K., Keeler, B.L., Powers, J.S., Stursova, M., Takacs-Vesbach, C., Waldrop, M.P., Wallenstein, M.D., Zak, D.R., Zeglin, L.H., 2008. Stoichiometry of soil enzyme activity at global scale. Ecol. Lett. 11, 1252–1264. https://doi.org/10.1111/j.1461-0248.2008.01245.x

Sinsabaugh, R.L., Repert, D., Weiland, T., Golladay, S.W., Linkins, A.E., 1991. Exoenzyme accumulation in epilithic biofilms. Hydrobiologia 222, 29–37. https://doi.org/10.1007/BF00017497

Smith, D.R., Warnemuende, E.A., Haggard, B.E., Huang, C., 2006. Changes in sediment–water column phosphorus interactions following sediment disturbance. Ecol. Eng. 27, 71–78. https://doi.org/10.1016/j.ecoleng.2005.10.013

Spilling, K., Piiparinen, J., Achterberg, E.P., Arístegui, J., Bach, L.T., Camarena-Gómez, M.T., Von Der Esch, E., Fischer, M.A., Gómez-Letona, M., Hernández-Hernández, N., Meyer, J., Schmitz, R.A., Riebesell, U., 2023. Extracellular enzyme activity in the coastal upwelling system off Peru: a mesocosm experiment. Biogeosciences 20, 1605–1619. https://doi.org/10.5194/bg-20-1605-2023

Tank, J.L., Rosi-Marshall, E.J., Griffiths, N.A., Entrekin, S.A., Stephen, M.L., 2010. A review of allochthonous organic matter dynamics and metabolism in streams. J. North Am. Benthol. Soc. 29, 118–146. https://doi.org/10.1899/08-170.1

Taylor, S., Saia, S.M., Buda, A.R., Regan, J.M., Walter, M.T., Carrick, H.J., 2022. Polyphosphate Accumulation Tracks Incremental P-Enrichment in a Temperate Watershed (Pennsylvania, United States) as an Indicator of Stream Ecosystem Legacy P. Front. Environ. Sci. 10, 920733. https://doi.org/10.3389/fenvs.2022.920733

Vannote, R.L., Minshall, G.W., Cummins, K.W., Sedell, J.R., Cushing, C.E., 1980. The River Continuum Concept. Can. J. Fish. Aquat. Sci. 37, 130–137. https://doi.org/10.1139/f80-017

Weitere, M., Altenburger, R., Anlanger, C., Baborowski, M., Bärlund, I., Beckers, L.-M., Borchardt, D., Brack, W., Brase, L., Busch, W., Chatzinotas, A., Deutschmann, B., Eligehausen, J., Frank, K., Graeber, D., Griebler, C., Hagemann, J., Herzsprung, P., Hollert, H., Inostroza, P.A., Jäger, C.G., Kallies, R., Kamjunke, N., Karrasch, B., Kaschuba, S., Kaus, A., Klauer, B., Knöller, K., Koschorreck, M., Krauss, M., Kunz, J.V., Kurz, M.J., Liess, M., Mages, M., Müller, C., Muschket, M., Musolff, A., Norf, H., Pöhlein, F., Reiber, L., Risse-Buhl, U., Schramm, K.-W., Schmitt-Jansen, M., Schmitz, M., Strachauer, U., Von Tümpling, W., Weber, N., Wild, R., Wolf, C., Brauns, M., 2021. Disentangling multiple chemical and non-chemical stressors in a lotic ecosystem using a longitudinal approach. Sci. Total Environ. 769, 144324. https://doi.org/10.1016/j.scitotenv.2020.144324

https://doi.org/10.5194/egusphere-2025-4844
Preprint. Discussion started: 10 October 2025

Wollschläger, U., Attinger, S., Borchardt, D., Brauns, M., Cuntz, M., Dietrich, P., Fleckenstein, J.H., Friese, K., Friesen, J., Harpke, A., Hildebrandt, A., Jäckel, G., Kamjunke, N., Knöller, K., Kögler, S., Kolditz, O., Krieg, R., Kumar, R., Lausch, A., Liess, M., Marx, A., Merz, R., Mueller, C., Musolff, A., Norf, H., Oswald, S.E., Rebmann, C., Reinstorf, F., Rode, M., Rink, K., Rinke, K., Samaniego, L., Vieweg, M., Vogel, H.-J., Weitere, M., Werban, U., Zink, M., Zacharias, S., 2017. The Bode hydrological observatory: a platform for integrated, interdisciplinary hydro-ecological research within the TERENO Harz/Central German Lowland Observatory. Environ. Earth Sci. 76, 29. https://doi.org/10.1007/s12665-016-6327-5

Xing, Y., Guo, L., Wang, Y., Zhao, Y., Jin, C., Gao, M., Ji, J., She, Z., 2021. An insight into the phosphorus distribution in extracellular and intracellular cell of Chlorella vulgaris under mixotrophic cultivation. Algal Res. 60, 102482. https://doi.org/10.1016/j.algal.2021.102482

Xu, Y., Wu, Y., Esquivel-Elizondo, S., Dolfing, J., Rittmann, B.E., 2020. Using Microbial Aggregates to Entrap Aqueous Phosphorus. Trends Biotechnol. 38, 1292–1303. https://doi.org/10.1016/j.tibtech.2020.03.012

Zhang, H.-L., Fang, W., Wang, Y.-P., Sheng, G.-P., Xia, C.-W., Zeng, R.J., Yu, H.-Q., 2013. Species of phosphorus in the extracellular polymeric substances of EBPR sludge. Bioresour. Technol. 142, 714–718. https://doi.org/10.1016/j.biortech.2013.05.068

Zhou, Y., Nguyen, B.T., Zhou, C., Straka, L., Lai, Y.S., Xia, S., Rittmann, B.E., 2017. The distribution of phosphorus and its transformations during batch growth of Synechocystis. Water Res. 122, 355–362. https://doi.org/10.1016/j.watres.2017.06.017